

# Shallow shadows: Expectation estimation using low-depth random Clifford circuits

Christian Bertoni,<sup>1</sup> Jonas Haferkamp,<sup>1</sup> Marcel Hinsche,<sup>1</sup> Marios Ioannou,<sup>1</sup> Jens Eisert,<sup>1,2,3</sup> and Hakop Pashayan<sup>1</sup>

<sup>1</sup>*Dahlem Center for Complex Quantum Systems, Freie Universität Berlin, Germany*

<sup>2</sup>*Helmholtz-Zentrum Berlin für Materialien und Energie, 14109 Berlin, Germany*

<sup>3</sup>*Fraunhofer Heinrich Hertz Institute, 10587 Berlin, Germany*

(Dated: September 28, 2022)

We provide practical and powerful schemes for learning many properties of an unknown  $n$ -qubit quantum state using a sparing number of copies of the state. Specifically, we present a depth-modulated randomized measurement scheme that interpolates between two known classical shadows schemes based on *random Pauli measurements* and *random Clifford measurements*. These can be seen within our scheme as the special cases of zero and infinite depth respectively. We focus on the regime where depth scales logarithmically in  $n$  and provide evidence that this retains the desirable properties of both extremal schemes whilst, in contrast to the random Clifford scheme, also being experimentally feasible. We present methods for two key tasks; estimating expectation values of certain observables from generated classical shadows and, computing upper bounds on the depth-modulated shadow norm, thus providing rigorous guarantees on the accuracy of the output estimates. We consider observables that can be written as a linear combination of  $\text{poly}(n)$  Paulis and observables that can be written as a low bond dimension matrix product operator. For the former class of observables both tasks are solved efficiently in  $n$ . For the latter class, we do not guarantee efficiency but present a method that works in practice; by variationally computing a heralded approximate inverses of a tensor network that can then be used for efficiently executing both these tasks.

## I. INTRODUCTION

Estimating properties of complex quantum systems is one of the core tasks of quantum mechanics. It has long been noted that recovering quantum states from access to a limited number of copies/samples is a demanding task for quantum systems involving a large number of degrees of freedom. Quantum state tomography and related approaches allow for the full recovery of unknown quantum states, but at the cost of enormous effort [1–5]. This can be seen as a road block in the study of quantum many-body systems and quantum simulation [6]. The presence of structure does lessen the burden to an extent [7], but one still commonly has to deal with sample complexities that scale exponentially with the system size. Nevertheless, recovering the full quantum state [8–11] may be unnecessary for many tasks, and shortcuts are surely conceivable.

Randomized measurement [9, 11–15] has emerged as a surprisingly powerful tool for estimating properties of quantum systems, encompassing schemes that permit the estimation of many expectation values from relatively few copies of the unknown quantum state. In a seminal work, Huang, Kueng and Preskill (HKP) proposed an approach based on so called *classical shadows* [11]. These are classical representations, obtained via suitable measurements, from which the expectation values of many observables can be estimated. Importantly, in contrast to Ref. [10], these classical shadows are obtained without prior knowledge of the specific choice of observables. Additionally, HKP provide rigorous performance guarantees based on what is called the shadow norm, thus permitting one to determine the trade-off between the number of samples and the accuracy of the estimated expectation value for any given observable.

The HKP classical shadows protocol has two variants; one randomizes the computational basis measurement by first applying a global Clifford unitary sampled uniformly at random

to each copy of the unknown quantum state (a.k.a. random Clifford measurements), the other by applying a layer of random single qubit Clifford gates (a.k.a. random Pauli measurements). Both prescriptions give rise to highly interesting and complementary schemes, each able to estimate expectation values for a large class of observables using a sparing number of copies of the unknown state. The global Clifford scheme performs well for observables with controlled Frobenius norm including quantum states (for fidelity estimation) and other low rank operators with bounded spectral norm. However, this scheme performs very poorly for high rank observables such as Pauli strings, even those with low weight. Additionally, already for states with a few qubits, the practical challenges associated with implementing this scheme are daunting. In contrast, the single qubit Clifford scheme is technologically far less demanding and has seen experimental implementation [16–18], however, it requires a number of samples that scales exponentially in the weight of the observable restricting its application to observables supported on a small number of qubits. To make the powerful global Clifford scheme into a tool useful in present-day laboratories and simultaneously endow it with the advantages of the single qubit Clifford scheme on local observables, it is key to identify and study a family of shadow schemes connecting these extremes.

A natural approach is to use randomized Clifford circuits modulated by circuit depth where the single qubit and global Clifford schemes of HKP can be seen as the zero and infinite depth extremes, respectively. However, intermediate schemes possess significant qualitative differences related to the fact that low depth Clifford circuits do not form a group. For intermediate schemes, two key technical challenges are

1. Inverting the channel associated with randomized measurements (a.k.a. the *measurement channel*) to permit the estimation of expectation values from shadows.
2. Bounding the shadow norms to obtain guarantees on the

accuracy of estimates.

These are closely related to sufficiently characterizing the second and third moment operators with respect to the (depth-modulated) Clifford ensembles, respectively. Accomplishing this is significantly more challenging for intermediate depths. For example, in the single qubit and global Clifford schemes of HKP, the measurement channel has a high degree of symmetry<sup>1</sup>, and it is simply the local and global depolarizing channel, respectively, making inversion simple. More generally, this channel is depth dependent and, in the intermediate regime away from these extremes, it loses some of its highly symmetric structure. A path to a practical, depth-modulated classical shadows scheme must overcome these obstacles.

Here, we present a practical, depth-modulated classical shadows scheme for low depths. We give methods for computing rigorous guarantees on the scheme's performance and discuss how the choice of depth and observable affects performance. More precisely, our protocol randomizes computational basis measurements using Clifford circuits of depth  $d \in \{\infty, 0, 1, 2, \dots\}$  generated by geometrically local, two-qubit Clifford gates acting on  $n$  qubits.

We then present numerical methods for either exactly computing or upper bounding the depth-dependent shadow norm associated with a given observable, permitting guarantees on the trade-off between the number of copies of the state used and the accuracy of the estimates. A key to our method is the probabilistic interpretation of the eigenvalues of the measurement channels and coefficients relevant in the computation of the shadow norm. This permits use of tensor networks to, efficiently in  $n$ , describe and manipulate key objects such as the measurement channel and the classical shadows.

We consider two observable input models, both supporting an efficient description. These are; observables given as a linear combination of at most  $\text{poly}(n)$  Paulis (we call these *sparse observables*) and observables given as a matrix product operator (MPO) with a  $\text{poly}(n)$  bounded bond dimension (we call these *shallow observables*). An example of the former is local Hamiltonians, an example of the latter is projectors onto Matrix Product States (MPS) for fidelity estimation. In the  $d \leq \mathcal{O}(\log n)$  regime, our scheme permits efficient estimation of expectation values and efficient computation of shadow norm bounds with respect to sparse observables. In the shallow observable input model, we require a  $\text{poly}(n)$  bond dimension matrix product state representation of the inverse measurement channel. Given this, efficient estimation of expectation values and efficient computation of shadow norm bounds is achieved. We employ a variational method for computing an approximate inverse to the measurement channel produced in the form of a low bond dimension MPS. This approximation error is bounded, permitting rigorous bounds on the errors associated with expectation value estimation. In practice, our variational inversion procedure

only needs to be executed once for any fixed depth  $d$  and system size  $n$  and works well for practically motivated parameter scales. However, for an arbitrary choice of parameters  $n$  and  $d$ , this procedure is not guaranteed to produce a high accuracy approximate inverse within a run-time that is feasible or efficient in system size.

Recently, sufficient assumptions on the unitary ensemble for shadow estimation were identified in Refs. [19, 20]: Meaningful estimates can be obtained from ensembles invariant under suitable local unitaries. In particular, Ref. [20] provides a general framework for *locally scrambling dynamics* based on entanglement features. In contrast, our work focuses on providing an explicit practical protocol for performing expectation estimation.

Our research was performed concurrently to that of Ref. [21] and their protocol overlaps significantly with ours. Nevertheless, our analysis goes further in some respects. Refs. [19–21] focus on the *entanglement features* formalism and the so called *locally scrambled shadow norm* which bounds the sample complexity for typical input states<sup>2</sup> (as opposed to worst case input states). This quantity is upper bounded by the shadow norm but is used as a proxy for the shadow norm since it is easier to characterize mathematically and, for certain observables, is expected to be proportional to the shadow norm based on numerical evidence. We present bounds for the *shadow norm*. Additionally, we present rigorous *analytical* upper bounds to the locally scrambled shadow norm in the regime  $d = \Theta(\log(n))$ . This provides evidence that this regime achieves an ideal middle ground between the  $d = 0$  and  $d = \infty$  cases in the following form. We show that for typical input states our  $d = \Theta(\log(n))$  protocol is expected to yield, up to constant factors, the same sample complexity as the much more experimentally demanding global Cliffords scheme. Additionally, we show that for the important class of observables that are sparse, have low-weight Pauli components and have  $\text{poly}(n)$  bounded Pauli coefficients (e.g., local Hamiltonians), in contrast to the global scheme, our  $d = \Theta(\log(n))$  scheme is provably sample efficient.

## II. NOTATION AND OVERVIEW

Throughout, we will use  $\mathbb{I}$ ,  $X$ ,  $Y$ , and  $Z$  to denote the single qubit Pauli operators, unless otherwise stated. We use  $\mathcal{P}_n := \{\mathbb{I}, X, Y, Z\}^{\otimes n}$  to denote the  $n$ -qubit set of Pauli strings (without phases). We index the element of  $\mathcal{P}_n$  by  $\lambda = (x, z) \in \{0, 1\}^n \times \{0, 1\}^n$  as follows

$$P^\lambda = \bigotimes_{j \in [n]} i^{x_j z_j} X^{x_j} Z^{z_j}, \quad (1)$$

<sup>1</sup> In the single qubit Clifford case, the measurement channel commutes with the canonical representation of the permutation group  $S_n$  and the Pauli group. In the global Clifford case, it commutes with any global Clifford.

<sup>2</sup> The locally scrambled shadow norm bounds the sample complexity averaged over all states in a one design, hence if it is bounded by some  $B > 0$ , for some  $\delta > 0$  a fraction  $1 - \delta$  of these states will have a sample complexity upper bounded by  $\sim B/\delta$ .

and use  $\pm \mathcal{Z}$  to denote  $\{\pm P^{(0^n, z)} \mid z \in \{0, 1\}^n\}$  i.e., the set of Pauli strings consisting only of  $\mathbb{I}$  and  $Z$  factors up to a phase factor of  $\pm 1$ . We use  $\mathcal{C}_n$  to denote the  $n$ -qubit Clifford group and  $\oplus$  to denote binary vector addition modulo 2.

In Section III, we give a brief summary of the method proposed in Ref. [11]. In Section IV, we sketch out our depth-modulated classical shadows method. In the subsequent sections we then go into more details regarding the ingredients of our scheme. In Sections V and VII, we give a conceptually valuable interpretation of the measurement channel's eigenvalues and suggest a technique for inverting it. In Section VI, we discuss the method of computing classical shadows and expectation values of observables from randomized measurements. Finally in Section VIII, we analyse the sample complexity of our method and provide numerical experiments in Section IX.

### III. THE HKP CLASSICAL SHADOWS PROTOCOL

Given many identical copies of an unknown  $n$ -qubit quantum state  $\rho$ , the goal is to compute a classical description  $\hat{\rho}$  such that for any observable  $O$  in a large class, the classical description can be used to generate sufficiently accurate expectation values. Ref. [11] defines an operator norm  $\|O\|_s$  and a procedure for computing a classical description  $\hat{\rho}$  (the shadow) from  $N$  copies of the unknown state  $\rho$ . In particular, the  $N$ -copy shadow can be thought of as a list of  $N$  independent copies each of which can be represented as a stabilizer state acted upon by the inverse of the measurement channel. After the shadow has been constructed, we are given a set of  $M$  distinct observables  $\{O_i\}_{i \in [M]}$  with spectrum in the interval  $[-1, 1]$  and bounded norm,  $\|O_i\|_s^2 \leq B$ . To estimate  $e_i := \text{tr}(O_i \rho)$ , the *median of means* method [22] is employed [11, 23].

Here, the 1-copy shadows are partitioned into equal sized blocks and averaged within each block to produce  $\hat{\rho}^{(j)}$  for each block  $j$ . The estimate  $\hat{e}_i$  is given by taking the median of  $\text{tr}(O_i \hat{\rho}^{(j)})$  values over all blocks. With this scheme, HKP show that a surprisingly small number of copies of  $\rho$  suffice to construct  $\hat{\rho}$  to sufficient accuracy such that for all  $M$  observables the expectation values with respect to  $\rho$  can be efficiently estimated from  $\hat{\rho}$ . More precisely, they show that with high probability over the randomness of the construction of the shadow,  $|e_i - \hat{e}_i| \leq \epsilon$  for all  $i \in [M]$  provided  $N \geq \Omega(B \log(M) \epsilon^{-2})$ .

To construct the shadow, for each copy of  $\rho$ , a unitary  $U \in \mathbb{U} \subseteq \mathcal{C}_n$  is independently chosen with probability  $\mu(U)$  from an ensemble of  $n$ -qubit Clifford gates  $\mathcal{U} = (\mathbb{U}, \mu)$ . From  $\rho$ , the state  $U \rho U^\dagger$  is generated and measured in the computational basis to produce some computational basis state  $|b\rangle\langle b|$ . Undoing the unitary  $U$  produces the stabilizer state  $\sigma = U^\dagger |b\rangle\langle b| U$ , also known as a *snapshot* of  $\rho$ . The expected outcome of this process (over the ensemble and measurement outcomes) can be viewed as a linear map, which we will refer

to as the *measurement channel*.

$$\mathcal{M}(\rho) := \mathbb{E}_{U \sim \mathcal{U}} \left[ \sum_{b \in \{0, 1\}^n} \langle b | U \rho U^\dagger | b \rangle U^\dagger |b\rangle\langle b| U \right]. \quad (2)$$

Assuming this channel,  $\mathcal{M}(\cdot)$  is invertible, the operator  $\mathcal{M}^{-1}(U^\dagger |b\rangle\langle b| U)$  defines a *1-copy shadow*. It is clear that the shadow (and hence also an average of independent shadows) is an unbiased estimator of  $\rho$  i.e., it reproduces  $\rho$  on expectation. Since expectation values are linear functions of  $\rho$ , a multi-copy average of shadows can be used as an unbiased estimator of expectation values; however, how quickly (in the number of copies) this estimate converges to the expectation value is determined by the variance of the estimator which is upper bounded by the squared shadow norm  $\|O\|_s^2$ ,

$$\max_{\sigma} \left\{ \mathbb{E}_{U \sim \mathcal{U}} \left[ \sum_{b \in \{0, 1\}^n} \langle b | U \sigma U^\dagger | b \rangle \langle b | U \mathcal{M}^{-1}(O) U^\dagger | b \rangle^2 \right] \right\}, \quad (3)$$

where the maximization is over density states  $\sigma$ .

We note that the procedure for constructing the shadow, the measurement channel and the shadow norm all depend on the choice of ensemble  $\mathcal{U}$ . Ref. [11] explicitly considers two ensembles we label as  $\mathcal{U}_0 = (\mathbb{U}_0, \mu_0)$  and  $\mathcal{U}_\infty = (\mathbb{U}_\infty, \mu_\infty)$  where  $\mathbb{U}_0$  consists of all  $n$ -fold tensor products of single qubit Clifford unitaries and  $\mathbb{U}_\infty$  consists of all  $n$ -qubit Clifford unitaries with  $\mu_0$  and  $\mu_\infty$  being the uniform distribution over  $\mathbb{U}_0$  and  $\mathbb{U}_\infty$ , respectively. Notice that linear depth circuits already suffice to implement  $\mathcal{U}_\infty$  for all practical purposes [24], despite the notation, but that  $d = \infty$  is the depth the gate-wise random ensembles we introduce require to generate uniform randomness *exactly*. In these two extremal settings, the measurement channels (denoted  $\mathcal{M}_0(\cdot)$  and  $\mathcal{M}_\infty(\cdot)$ ) have a particularly simple form; acting as the product of single qubit depolarizing channels and a global depolarizing channel, respectively. That is, for  $P \neq \mathbb{I}$  an  $n$ -qubit Pauli, these act as

$$\mathcal{M}_0(P) = 3^{-|P|} P \quad \text{and} \quad \mathcal{M}_\infty(P) = \frac{1}{2^n + 1} P, \quad (4)$$

where  $|P| \in \{0, 1, \dots, n\}$  denotes the weight of the Pauli, i.e., the number of non-identity tensor factors. More generally, the action of the measurement channel can be defined by linear extension from Equation (4). Combined with the observation that  $\mathcal{M}_0(\mathbb{I}^{\otimes n}) = \mathbb{I}^{\otimes n} = \mathcal{M}_\infty(\mathbb{I}^{\otimes n})$ , Equation (4) also establishes that these measurement channels are invertible.

### IV. OVERVIEW OF THE METHOD

In this section we give a step by step overview of how our method can be implemented.

## Depth-modulated classical shadows

- Given  $N$  copies of some state  $\rho$  on  $n$  qubits, pick  $d$ . We expect the ideal  $d$  to scale like  $\log(n)$ , both in terms of efficiency of implementation and in terms of sample efficiency for the widest possible class of observables.
- Construct the MPS representation of the measurement channel  $\mathcal{M}_d$  as per Section V.
- Sample the  $N$  classical shadows as per Section VI.
- Choose a set of observables. If there are any shallow observables, obtain an MPS representation of  $\mathcal{M}_d^{-1}$  as per Section VII.
- Compute the corresponding expectation values as per Section VI.
- Upper bound the shadow norms of the chosen observables as per Section VIII.
- Use standard techniques to bound the accuracies of estimates from upper bounds on the variances of the unbiased estimators.

## V. REPRESENTATIONS OF THE MEASUREMENT CHANNEL

We consider the extension of the classical shadows protocol to the intermediate Clifford depth regime. Concretely, for ‘circuit depth’  $d \in \{\infty, 0, 1, \dots\}$ , we define  $\mathcal{U}_d = (\mathbb{U}_d, \mu_d)$  as the ensemble of Clifford unitaries constructed by first applying a uniformly random single qubit Clifford gate to each qubit (the 0<sup>th</sup> layer)<sup>3</sup> then for each layer  $i \in [d]$  we apply uniformly randomly chosen two qubit Clifford gates in a nearest-neighbour circular brickwork pattern applied to  $n$  (even) qubits in a circle, i.e., the first and last qubit are identified as neighbours (see Fig. 1). With some modifications, our work generalizes to qubits on a line (non-circular), arbitrary  $n$  and to other architectures but we do not consider these here for clarity and concreteness. We note that (for  $n$  even), the  $d = 0$  and  $d = \infty$  limits of our ensembles  $\mathcal{U}_d$  recover the  $\mathcal{U}_0$  and  $\mathcal{U}_\infty$  ensembles studied in Huang et. al. In fact, for  $d = \mathcal{O}(n)$ ,  $\mathcal{U}_d$  becomes an approximate 3-design [24] and recovers the properties of  $\mathcal{U}_\infty$  for our purposes. Using Equations (2) and (3), we define the measurement channel  $\mathcal{M}_d(\cdot)$  and  $\|\cdot\|_{s(d)}$  with respect to the ensemble  $\mathcal{U}_d$ .

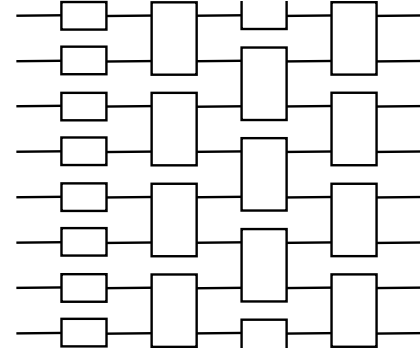


FIG. 1. Nearest-neighbour circular brickwork architecture for  $n = 8$  qubits and depth  $d = 3$ . Consists of 3 layers (excluding) the 0<sup>th</sup> layer of single qubit gates. The second layer contains a two qubit gate acting on qubits 1 and 8 which are identified as nearest-neighbour in this architecture.

**Lemma 1.** For  $\lambda \in \{0, 1\}^{2n}$ , let  $t_{\lambda, d} \in [0, 1]$  be defined as

$$t_{\lambda, d} := \Pr_{U \sim \mathcal{U}_d} (UP^\lambda U^\dagger \in \pm \mathcal{Z}), \quad (5)$$

then,

$$\mathcal{M}_d(P^\lambda) = t_{\lambda, d} P^\lambda. \quad (6)$$

The proof of Lemma 1 can be found in Appendix A. We note that the diagonal action of the measurement channel in the Pauli basis was independently identified in Ref. [19]. This probabilistic interpretation has an important conceptual value as it allows to interpret  $t_{\lambda, d}$  as the probability of a certain outcome of a classical random walk on bit strings, rather than on the Clifford group. As a matter of fact since our ensemble is invariant under local Cliffords  $t_{\lambda, d}$  only depends on the support of  $P^\lambda$ . To recover Eq. (4) from Lemma 1, we make the trivial observation that  $U \in \mathbb{U}_0$  must preserve Pauli weight, i.e.,  $|P| = |UPU^\dagger|$  sending each single qubit non-identity tensor factor of  $P$  to  $\pm Z$  with probability 1/3, hence,  $t_{\lambda, 0} = 3^{-|P^\lambda|}$ . Further, for  $U \sim \mathcal{U}_\infty$  and  $P^\lambda \neq \mathbb{I}^{\otimes n}$ , the Pauli  $UP^\lambda U^\dagger$  is equally likely to be any non-identity Pauli giving

$$t_{\lambda, \infty} = \frac{2^n - 1}{4^n - 1} = \frac{1}{2^n + 1}.$$

We now present efficient methods for exactly computing both  $t_{\lambda, d}$  for a given  $\lambda$  and  $\mathcal{M}_d(\sigma)$  for a state  $\sigma$  given as a low<sup>4</sup> bond dimension MPO provided that  $d = \mathcal{O}(\log(n))$ . The way in which we resort to tensor network techniques to arrive at scalable randomized schemes for quantum systems identification is reminiscent of that of Ref. [9]. We will work in the Pauli basis  $\mathcal{P}_n$  as it diagonalizes the measurement channel (c.f. Equation (6)).

Any operator  $\sigma$  acting on  $(\mathbb{C}^2)^n$  can be written in the Pauli basis as

$$\sigma = \sum_{\lambda} \alpha_{\lambda} P^\lambda, \quad (7)$$

<sup>3</sup> Strictly speaking, this first layer does not change the ensemble and can be omitted, we include it here as then the  $d = 0$  case of our ensemble corresponds to the random Pauli measurements scheme of [11].

<sup>4</sup> Meaning, upper bounded by  $\text{poly}(n)$ .

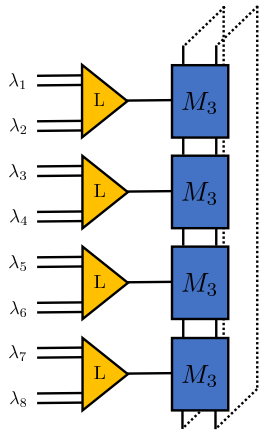


FIG. 2. Tensor network for computing  $t_{\lambda,d}$  for  $n = 8$  qubits and depth  $d = 3$ . Each  $L$  tensor is a logical operator taking the OR of two NOR gates. The  $M_d$  tensors can be constructed from the random Clifford architecture (c.f. Figure 1) as per Appendix B. When its horizontal leg input value  $h \in \{0, 1\}$  is assigned, the tensor becomes a transfer matrix  $M_{d,h}$  of dimension  $2^{d-1} \times 2^{d-1}$ .

with the coefficients  $\alpha_\lambda$  in the form

$$\alpha_\lambda = \text{tr}(C_{\lambda_1} C_{\lambda_2} \cdots C_{\lambda_n}), \quad (8)$$

where  $C_{0,0}, \dots, C_{1,1}$  are  $b_\alpha \times b_\alpha$  matrices and  $b_\alpha$  is known as the bond dimension of the vector  $\alpha_\bullet$ . We will be interested in operators  $\sigma$  such that the bond dimension is at most polynomial in  $n$ . In general, a bond dimension that scales exponentially in  $n$  is needed to express an arbitrary operator via Equation (8). Equation (8) takes the form of a matrix product state. This form is particularly useful since contractions over exponentially many indices can be computed efficiently. For example,

$$\sum_\lambda \alpha_\lambda = \text{tr} \left( \left( \sum_{\lambda_1} C_{\lambda_1} \right) \times \dots \times \left( \sum_{\lambda_n} C_{\lambda_n} \right) \right) \quad (9)$$

with the right hand side being efficiently computable in  $n$ . By Equation (6), we have

$$\mathcal{M}_d(\sigma) = \sum_\lambda \alpha_\lambda t_{\lambda,d} P^\lambda, \quad (10)$$

We will write the vector  $t_{\bullet,d}$  as an MPS. We note that if the bond dimensions of  $\alpha_\bullet$  and  $t_{\bullet,d}$  are  $n^{\mathcal{O}(1)}$  then  $\mathcal{M}_d(\sigma)$  can be written as an MPO with  $n^{\mathcal{O}(1)}$  bond dimension. In particular, the updated vector of Pauli coefficients  $\alpha'_\bullet$  can be written as an MPS with bond dimension that is the product of the bond dimensions of  $\alpha_\bullet$  and  $t_{\bullet,d}$  where  $\alpha'_\lambda := \alpha_\lambda t_{\lambda,d}$ . This will permit the efficient computations of expectation values with respect to  $n^{\mathcal{O}(1)}$  bond dimension MPO observables

**Lemma 2.**  $t_{\lambda,d}$  can be written as an MPS with bond dimension at most  $2^{d-1}$ .

We present the proof of Lemma 2 in Appendix B where we show that  $t_{\lambda,d}$  is given as the tensor element depicted in Figure 2. Algebraically,  $t_{\lambda,d}$  can be written in MPS form as

$$t_{\lambda,d} = \text{tr}(M_{d,h_1} M_{d,h_2} \cdots M_{d,h_{n/2}}), \quad (11)$$

where  $g_j := \text{NOR}(\lambda_j)$ ,  $h_j := \text{OR}(g_{2j-1}, g_{2j})$  and the matrices  $M_{d,0}$  and  $M_{d,1}$  are  $2^{d-1} \times 2^{d-1}$  real matrices with their explicit construction given in Appendix B. We write  $\mathcal{M}_d(\sigma)$  as an MPO as follows

$$\mathcal{M}_d(\sigma) = \sum_\lambda \text{tr} \left( M_{d,h_1} \otimes C'_1 \times \dots \times M_{d,h_{n/2}} \otimes C'_{n/2} \right) P^\lambda, \quad (12)$$

where  $C'_j := C_{\lambda_{2j-1}} C_{\lambda_{2j}}$  and we note that both  $C'_j$  and  $M_{d,h_j}$  depend on  $\lambda_{2j-1}$  and  $\lambda_{2j}$ .

**Corollary 3.** For depth  $d = \mathcal{O}(\log n)$ , the probabilities  $t_{\lambda,d}$  can be exactly computed in run-time  $n^{\mathcal{O}(1)}$ .

The proof is clear from Equation (11). For the shadow protocol to work, it is essential that the measurement channel is invertible. From Equation (5), we observe that for any  $\lambda \in \{0, 1\}^{2n}$ , the probability  $t_{\lambda,d}$  is non-zero ensuring non-singularity and that the inverse is given by

$$\mathcal{M}_d^{-1}(P^\lambda) = \frac{1}{t_{\lambda,d}} P^\lambda. \quad (13)$$

With the application of Corollary 3, this form can be useful in the computation of  $\mathcal{M}_d^{-1}(\sigma)$  for a  $\sigma$  with a sparse representation in the Pauli basis, i.e., where at most  $n^{\mathcal{O}(1)}$  of the Pauli coefficients are non-zero, which is necessary for the estimation of expectation values as we will shortly show. However, in the more general setting we wish to represent  $1/t_{\lambda,d}$  as an MPS and  $\mathcal{M}_d^{-1}(\sigma)$  as an MPO analogously to Equation (12), we will do this in Section VII.

## VI. COMPUTING SHALLOW SHADOWS AND ESTIMATING EXPECTATION VALUES

We now specify how copies of the unknown  $\rho$  are measured and stored in a form that specifies the shadow  $\hat{\rho}$ . This step of our procedure is analogous to Ref. [11]. That is, to compute a single shadow, we first sample  $U \sim \mathcal{U}_d$  and apply  $U$  to a copy of  $\rho$ . We then measure in the computational basis. The output computational basis state  $|b\rangle\langle b|$  is then conjugated by  $U^\dagger$  to produce a snapshot  $\sigma = U^\dagger |b\rangle\langle b| U$  that depends on the random variables  $U$  and  $b$ . The rest of the procedure is based on the fact that the expected value of  $\sigma$  is by definition  $\mathcal{M}_d(\rho)$  (cf. Equation (2)), hence the expectation value of  $\mathcal{M}_d^{-1}(\sigma)$  is  $\rho$ .  $\mathcal{M}_d^{-1}(\sigma)$  is then an unbiased estimator of  $\rho$ . As the trace is linear, for any observable  $O$ , we then get that  $\text{tr}(O \mathcal{M}_d^{-1}(\sigma))$  is an unbiased estimator of the expectation value  $\text{tr}(O \rho)$ . We note here that since  $\mathcal{M}_d^{-1}$  is self adjoint,  $\text{tr}(\mathcal{M}_d^{-1}(O) \sigma)$  is an unbiased estimator of  $\text{tr}(O \rho)$  as well. To estimate  $\text{tr}(\rho O)$  we then have to efficiently sample and store a large number of instances of this estimator, the sample efficiency of the estimation depends on its second moment, the shadow norm, which we discuss in Section VIII. At this point the procedure is different depending on the type of observables. If  $O$  is a sparse observables, we have access to an efficient description

of  $O$  in terms of Paulis, meaning that we have

$$O = \sum_{k=1}^r \beta_{\lambda_r} P^{\lambda_r} \quad (14)$$

with  $r \leq n^{\mathcal{O}(1)}$ . We can then efficiently compute  $t_{\lambda_r, d}$  for each  $r$  and simply store the inverted observable

$$\mathcal{M}_d^{-1}(O) = \sum_{k=1}^r \frac{\beta_{\lambda_r}}{t_{\lambda_r, d}} P^{\lambda_r}. \quad (15)$$

Computing the expectation value is now simply a matter of efficiently computing  $\langle b | U P^{\lambda_r} U^\dagger | b \rangle$  for every snapshot, which can be done efficiently as  $U | b \rangle$  is a stabilizer state.

If instead  $O$  is a *shallow* observable, it is given as

$$O = \sum_{\lambda} \beta_{\lambda} P_{\lambda} \quad (16)$$

where  $\beta_{\lambda}$  is representable an MPS with low bond dimension, or equivalently  $O$  might be represented as an MPO in any local basis, since local basis changes do not affect the bond dimension. For example  $O$  might be a rank one projector corresponding to an MPS state. In this case, it is necessary to construct an MPS representation for  $\mathcal{M}_d^{-1}(\bullet)$  as described in Section VII. We note that since  $|b\rangle$  is a product state vector and  $U \in \mathbb{U}_d$  is depth  $d$ , the stabilizer state  $\sigma$  can be written as an MPO (c.f. Equation (7)) with bond dimension  $b_{\alpha} \leq 4^{d-1}$ . Depending on the relative number of observables to estimate and snapshots stored, it might be more efficient to use tensor contractions to store either  $\mathcal{M}_d^{-1}(\sigma)$  for every snapshot  $\sigma$  or  $\mathcal{M}_d^{-1}(O)$  for every observable  $O$  we are interested in. In any case, for every snapshot  $\sigma$  we can then efficiently compute  $\text{tr}(O \mathcal{M}_d^{-1}(\sigma))$  by contracting the tensor networks corresponding to  $O$ ,  $\sigma$ , and  $\mathcal{M}_d^{-1}(\bullet)$ .

## VII. HERALDED MATRIX PRODUCT OPERATOR INVERSION

We present a variational method inspired by Ref. [25] for computing two matrices  $V_0$  and  $V_1$ . These parametrise an MPS that approximates  $1/t_{\lambda, d}$  on all inputs  $\lambda$  via

$$v(P^{\lambda}) = \text{tr}(V_{h_1} V_{h_2} \cdots V_{h_{n/2}}), \quad (17)$$

where the  $h_j$  are the same functions of  $\lambda$  used in Equation (11). The outputs of Equations (11) and (17) depend on  $\lambda$  indirectly through their dependence on  $h(\lambda)$ . In this section, we will only be interested in the dependence of their output on  $h \in \{0, 1\}^{n/2}$ . For simplicity of notation we fix  $d$  and use  $t(x)$  and  $v(x)$  to denote the left hand side of these equations in the case  $h(\lambda) = x$ .

Our procedure works by choosing two  $b_v \times b_v$  matrices  $V_0, V_1$  (initially  $b_v = 1$ ) then efficiently evaluating a cost function

$$\begin{aligned} c(V_0, V_1)^2 &:= \sum_x |t(x)v(x) - 1|^2 \\ &= \sum_x |t(x)v(x)|^2 - 2\text{Re}(t(x)v(x)) + 1 \end{aligned} \quad (18)$$

using Equation (9). Through a variational method, we minimize the cost function and if the cost is still unacceptably large, we increment  $b_v$  by 1 and repeat. Our procedure is not guaranteed to reach a small cost value within a feasible run-time, however, we have observed our method to work for small values of  $d$ , i.e.,  $d = 3$  and  $d = 4$  without resorting to high performance computing. In Appendix C, we present a  $V_0$  and  $V_1$  with  $c(V_0, V_1) \leq 10^{-5}$  for  $n = 8$  and  $d \in \{2, 3, 4\}$ . As an example, the  $d = 3$  matrices were found within approximately 1 minute on a laptop computer and have a bond dimension of  $b_v = 3$ , which is smaller than the bond dimension associated with the measurement channel ( $2^{d-1} = 4$ ).

We point out some key features of our protocol. First, our procedure is heralded in the sense that if the procedure finds a  $V_0$  and  $V_1$  with a small cost function, then we are guaranteed that this can be used to produce expectation value estimates with negligible error arising from this approximate inverse procedure. In fact, while the cost function in Section VII is easy to compute, it is expected that the actual error given by the approximation should be smaller, since it scales like  $\max_x |t(x)v(x) - 1|$  instead. We prove the following in Appendix D:

**Lemma 4.** *Let  $\mathcal{V}$  be a channel that is diagonal in the Pauli basis with coefficients  $v_{\lambda}$  for each  $P^{\lambda} \in \mathcal{P}_n$  and is an approximate inverse of the measurement channel in the sense that there exists  $\epsilon > 0$  such that for all  $\lambda \in \{0, 1\}^{2n}$ ,  $|1 - t_{\lambda, d} v_{\lambda}| \leq \epsilon$ . Then*

$$|\tilde{o} - \text{tr}(O\rho)| \leq \epsilon \|O\|_{\infty} \quad (19)$$

where  $\tilde{o}$  is the expectation value obtained by using the approximate inverse channel in the shadow protocol.

Second, we note that for a given  $n$  and  $d$ , the computation of a high accuracy variational inverse is only needed once. Hence, its run-time is a one-off cost for each new  $n, d$  pair.

## VIII. PERFORMANCE GUARANTEES

Shadow estimation is useful only insofar as the number of samples one needs to get to obtain a good estimate is well behaved, and in practice one needs to be able to estimate the number of samples needed to achieve a certain accuracy. For these purposes, the main quantity of interest is the shadow norm. For a given observable  $O$ , its shadow norm upper bounds the second moment (and hence also the variance) of the estimator  $\text{tr}(\hat{\rho}O)$  where  $\hat{\rho}$  is a random one copy shadow. In this section, unless otherwise stated, we will always assume  $d \leq \mathcal{O}(\log n)$ . We first present methods for computing upper bounds on the shadow norm of various classes of observables.

In particular we show how to exactly and efficiently compute the shadow norm of a Pauli operator, how to efficiently compute upper bounds on the shadow norm of a sparse operator and, how to efficiently compute upper bounds on the shadow norm of a shallow observable given an approximate inverse to the measurement channel in the form of a low bond dimension MPS.

We also consider the important sub-set of sparse operators that can be written as a linear combination of  $\mathcal{O}(\log n)$  weight Pauli operators with coefficients of size at most  $n^{\mathcal{O}(1)}$  such as, e.g., local Hamiltonians in variational schemes. We show a key result that all such observables have an  $n^{\mathcal{O}(1)}$  shadow norm and hence also an  $n^{\mathcal{O}(1)}$  sample complexity when  $d = \Theta(\log n)$ . We go on to give further evidence that the  $d = \Theta(\log n)$  regime achieves the “sweet spot” between the  $d = 0$  and  $d = \infty$  schemes of HKP in the sense that it permits the broadest class of observables that admit an  $n^{\mathcal{O}(1)}$  shadow norm.

Let us start by defining the *state dependent shadow norm*  $\|O\|_{s(d),\rho}^2$

$$\mathbb{E}_{U \sim \mathcal{U}_d} \left[ \sum_{b \in \{0,1\}^n} \langle b | U \rho U^\dagger | b \rangle \langle b | U \mathcal{M}^{-1}(O) U^\dagger | b \rangle^2 \right].$$

This is simply the second moment of the estimator of  $\text{tr}(\rho O)$ . Since  $\rho$  is unknown, the shadow norm  $\|O\|_{s(d)}$  is obtained by maximizing over all states  $\rho$ , i.e., by considering the worst possible variance. We can also define the *locally scrambled shadow norm* [19, 20] as the average, rather than the maximization, over all states in a state one-design, i.e., any ensemble of states  $\mathcal{E}$  such that  $\mathbb{E}_{\sigma \sim \mathcal{E}} [\sigma] = \mathbb{I}/2^n$ , as

$$\|O\|_{s(d),\text{LS}}^2 := \mathbb{E}_{\sigma \sim \mathcal{E}} \left[ \|O\|_{s(d),\sigma}^2 \right]. \quad (20)$$

This quantity can be interpreted as quantifying the average performance of the scheme, i.e., the performance for a “typical state”. We show that all of these objects are actually norms in Appendix F. The goal is now to present methods to efficiently compute upper bounds for the shadow norm. The following quantity, a higher order analogue to  $t_{\lambda,d}$ , will be central for this task. For  $\lambda, \lambda' \in \{0,1\}^{2n}$ , we define

$$\tau_{(\lambda,\lambda'),d} := \Pr_{U \sim \mathcal{U}_d} \left( UP^\lambda U^\dagger, UP^{\lambda'} U^\dagger \in \pm \mathcal{Z} \right). \quad (21)$$

That is,  $\tau_{(\lambda,\lambda'),d}$  is the probability that  $U$  sampled from the ensemble  $\mathcal{U}_d$  will map both Paulis  $P^\lambda$  and  $P^{\lambda'}$  to a tensor product of  $\mathbb{I}$  and  $Z$  operators up to a factor  $\pm 1$ . We present some useful properties of  $\tau_{(\lambda,\lambda')}$  in Appendix F, Lemma 15.

**Lemma 5.**  $\tau_{(\lambda,\lambda'),d}$  can be written as an MPS with bond dimension  $2^{\mathcal{O}(d)}$

The proof is presented in Appendix E, the next result follows immediately:

**Corollary 6.** For depth  $d = \mathcal{O}(\log n)$ , the probabilities  $\tau_{(\lambda,\lambda'),d}$  can be exactly computed in run-time  $n^{\mathcal{O}(1)}$ .

We now give a useful expression for the state dependent shadow norm:

**Theorem 7.** For any observable  $O$  with Pauli decomposition  $O = \sum_{\lambda} \beta_{\lambda} P^{\lambda}$  and any state  $\sigma$ , the square of the state dependent shadow norm is given by

$$\|O\|_{s(d),\sigma}^2 = \|O\|_{s(d),\text{LS}}^2 + \text{tr} \left( \sigma \tilde{O} \right) \quad (22)$$

where

$$\tilde{O} = \sum_{\lambda', \lambda \in \{0,1\}^{2n} : \lambda' \neq \lambda} P^{\lambda} P^{\lambda'} \beta_{\lambda} \beta_{\lambda'} \frac{\tau_{(\lambda,\lambda'),d}}{t_{\lambda,d} t_{\lambda',d}}. \quad (23)$$

Furthermore,

$$\|O\|_{s(d),\text{LS}}^2 = \sum_{\lambda \in \{0,1\}^{2n}} \frac{\beta_{\lambda}^2}{t_{\lambda,d}}. \quad (24)$$

We present the proof in Appendix F. We isolate the identity component of  $\sigma$  from the rest, as this gives rise to the locally scrambled shadow norm and in the  $d = \infty$  case this is the dominant term. Given access to low bond dimension MPS representations of  $\beta_{\bullet}$  and  $1/t_{\bullet,d}$ , the locally scrambled shadow norm can be efficiently computed exactly. We can immediately see that if the observable is a single Pauli, the second term  $\text{tr} \left( \sigma \tilde{O} \right)$  vanishes.

**Corollary 8.** For  $\lambda \in \{0,1\}^{2n}$ , the squared shadow norm of  $P^{\lambda}$  is

$$\|P^{\lambda}\|_{s(d)}^2 = \|P^{\lambda}\|_{s(d),\text{LS}}^2 = \frac{1}{t_{\lambda,d}}.$$

Hence, for  $d = \mathcal{O}(\log n)$  and  $d = \infty$ , all Pauli shadow norms can be efficiently calculated using Corollary 3 and Corollary 8. In this regime we can rigorously upper bound the shadow norm of certain linear combinations of Paulis, the following is a simple consequence of Theorem 11, which we will present at the end of this section, the triangle inequality and Corollary 8,

**Theorem 9.** Let  $O = \sum_{k=0}^r \beta_{\lambda_k} P^{\lambda_k}$  be a linear combination of Pauli operators such that each Pauli is supported on a region of length upper bounded by  $\mathcal{O}(\log(n))$ , then if  $d \leq \mathcal{O}(\log(n))$

$$\|O\|_{s(d)} \leq n^{\mathcal{O}(1)} \sum_{k=0}^r |\beta_{\lambda_k}|. \quad (25)$$

Beyond single Pauli operators, an important case in which the above is useful is local Hamiltonians, for which  $\sum_{k=0}^r |\beta_{\lambda_k}| \leq n^{\mathcal{O}(1)}$ , we then find that at logarithmic depth polynomially many samples are still sufficient to estimate local Hamiltonians to arbitrary precision, a property that is lost at  $d = \infty$ . For this class of observables, we note that both the estimation of expectation given a shadow and the computation of a polynomial upper bound on the shadow norm can

be computed efficiently and without the use of an approximate variational inverse.

It is worth noticing that the full expression of Equation (22) is simply

$$\|O\|_{s(d),\sigma}^2 = \text{tr} \left( \sigma \sum_{\lambda,\lambda'} \beta_\lambda \beta_{\lambda'} \frac{\tau_{(\lambda,\lambda'),d}}{t_{\lambda,d} t_{\lambda',d}} P^\lambda P^{\lambda'} \right). \quad (26)$$

For sparse observables Equation (26) may lend itself to numerical optimisation techniques. More generally, upper bounds on the second term in Equation (22) may be useful.

**Lemma 10.** *The following bounds hold for any observable*

$$\|O\|_{s(d)} \leq \sum_{\lambda} \frac{\beta_\lambda^2}{t_{\lambda,d}} + 2^{n/2} \sqrt{\sum_{\lambda \neq 0} \left| \sum_{\lambda'} \beta_{\lambda \oplus \lambda'} \beta_\lambda \frac{\tau_{(\lambda,\lambda'),d}}{t_{\lambda,d} t_{\lambda',d}} \right|^2}, \quad (27)$$

$$\begin{aligned} \|O\|_{s(d)} &\leq \sum_{\lambda} \frac{\beta_\lambda^2}{t_{\lambda,d}} + \sum_{\lambda \neq 0} \left| \sum_{\lambda'} \beta_{\lambda \oplus \lambda'} \beta_\lambda \frac{\tau_{(\lambda,\lambda'),d}}{t_{\lambda,d} t_{\lambda',d}} \right| \\ &\leq \sum_{\lambda,\lambda'} |\beta_\lambda| |\beta_{\lambda'}| \frac{\tau_{(\lambda,\lambda'),d}}{t_{\lambda,d} t_{\lambda',d}} \end{aligned} \quad (28)$$

These are, of course, not the tightest bounds one can get, but given a low bond dimension MPS representation of  $1/t_{\bullet,d}$  and  $\beta_\bullet$ , the first bound can be efficiently approximately<sup>5</sup> evaluated through tensor contractions, and similarly for the looser version of the second bound, given access to a low bond dimension MPS for  $|\beta_\bullet|$ . All three bounds can be computed for sparse observables. It is worth pointing out that in Equation (27) the bond dimensions of the quadratic and quartic components ( $\tau_{(\bullet),d}$ ,  $\beta_\bullet$  and  $v_\bullet$ , respectively) conspire to render the contraction infeasible beyond very small depths. We expect a significant reduction to this bond dimension is possible but leave this to future work. The proofs are given in Appendix F.

In addition to being able to compute the shadow norm for specific observables, it would be desirable to be able to determine whether the shallow shadows protocol is efficient for a determinate observable based on coarser properties, and in general, whether it is reasonable to expect that our protocol is useful in the regime in which it is efficient, i.e., logarithmic depth. In Ref. [11], the shadow norm of general observables was computed for the cases  $d = 0$  and  $d = \infty$ . In particular, it was found that for  $d = \infty$ , the shadow norm of  $O$  is proportional to its Frobenius norm, which makes it ideal for estimating fidelities of quantum states or more generally expectation values of low rank observables with bounded operator norm, but not for local observables or high rank operators such as Pauli strings, which have exponentially large

Frobenius norm. By contrast, the shadow norm of local operator is well behaved for  $d = 0$ . We provide evidence for and conjecture that a logarithmic depth circuit is the ideal middle ground between these two extremes, capturing enough of the long range entanglement to estimate global observables, while not losing so much local information. To fully prove this claim, one would need to analytically compute the shadow norm of a general observables, which, being a third moment of the circuit, is challenging. As evidence for this claim, we instead present rigorous *analytic* bounds on the locally scrambled shadow norm. This quantity is clearly upper bounded by the shadow norm,  $\|O\|_{s(d),\text{LS}} \leq \|O\|_{s(d)}$ , nevertheless in the extreme case  $d = \infty$  it exhibits the same scaling [11]. While not providing a worst case performance guarantee, we can interpret the value of  $\|O\|_{s(d),\text{LS}}^2$  being low as a reassurance that for a significant portion of states the protocol is sample efficient, and hence as supporting evidence for our initial claim. More specifically, if the locally scrambled shadow norm of an observable is smaller than some bound  $B$ , by Markov's inequality we can conclude that for a fraction  $1 - \delta$  of all states in any 1 design, its shadow norm is smaller than  $B/\delta$ . In Appendix H we employ recently developed methods for the anti-concentration of random quantum circuits to bound the locally scrambled shadow norm [26–28]. In particular, the locally scrambled shadow norm reduces to so-called second moments over the ensemble of random 2-local circuits. Using Weingarten calculus, we map these second moments to a partition function of an effective statistical mechanics model. We find the following theorem:

**Theorem 11.** *If  $d = \Theta(\log(n))$ , we have for any traceless observable  $O$*

$$\|O\|_{s(d),\text{LS}}^2 \leq 2\|O\|_F^2 \left( 1 + \frac{1}{n^{\mathcal{O}(1)}} \right). \quad (29)$$

Furthermore, let  $l$  be the maximum distance between two sites on which  $O$  is supported, if  $l \leq \mathcal{O}(\log(n))$ ,

$$\|O\|_{s(d),\text{LS}}^2 \leq n^{\mathcal{O}(1)} 2^{-n} \|O\|_F^2. \quad (30)$$

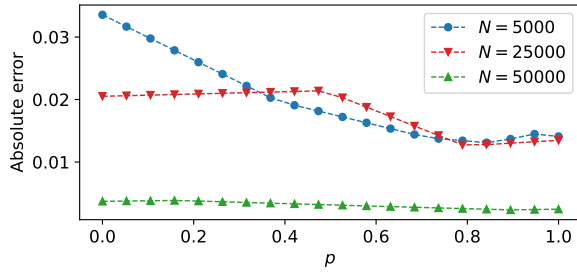
The constants and precise expressions are given in the proofs. The first bound in this theorem shows that for a large fraction of input states, a logarithmic depth shallow shadows scheme is sufficient to achieve the same sample efficiency as the global Clifford scheme of HKP (as in this case for traceless  $O$ ,  $\|O\|_F^2 \leq \|O\|_{s(\infty)}^2 \leq 3\|O\|_F^2$ , see [11]), up to a small correction which vanishes as the system size grows. The second bound shows that despite this, some of the desirable properties of the  $d = 0$  case are preserved up to and including logarithmic depth, namely, the sample complexity for local observables does not, for typical input states, grow exponentially in the system size.

## IX. NUMERICS

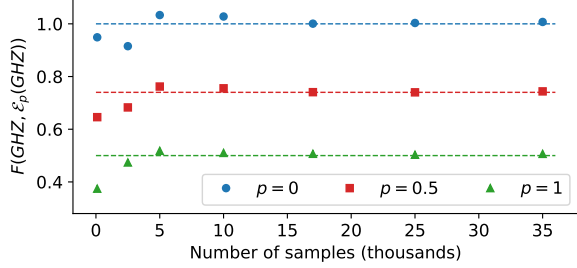
We now apply our protocol to some simple examples. In this section with fix  $n = 8$  qubits and a depth  $d = 3$ . All

<sup>5</sup> The approximation error arises from the use of the variational inverse but since this error is upper bounded, the shadow norm can in turn be upper bounded.

estimations are obtained via the median of means of 9 blocks comprising the total number of samples. When we compare estimates based on different numbers of snapshots,  $N$ , each group of snapshots is independently generated. However, when for a fixed  $N$ , we compare different observables, the same group of  $N$  snapshots is used to compute all observables. Thus, as per the HKP schemes, for a fixed shadow, we expect similar observables to have correlated errors in their estimated expectation values. We start with two different examples of low Frobenius norm observables. These are observables for which the  $d = \infty$  protocol would be ideal. In Figure 3, we show the absolute error of Shadow estimation of the fidelity of the *Greenberger-Horne-Zeilinger* (GHZ) state with a noisy GHZ state  $\mathcal{E}_p(\text{GHZ})$  where  $\mathcal{E}_p : \rho \mapsto (1-p)\rho + p \text{tr}_1(\rho)\mathbb{I}/2$  is the depolarizing channel on the first qubit for different values of  $p \in [0, 1]$  and different values of the number of samples  $N$ .



(a)

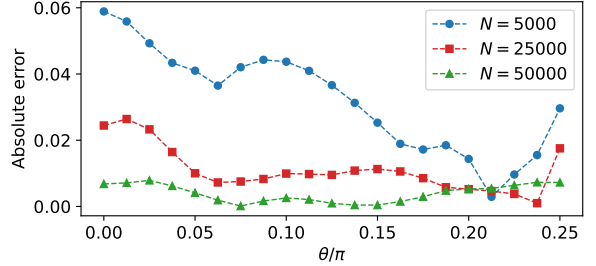


(b)

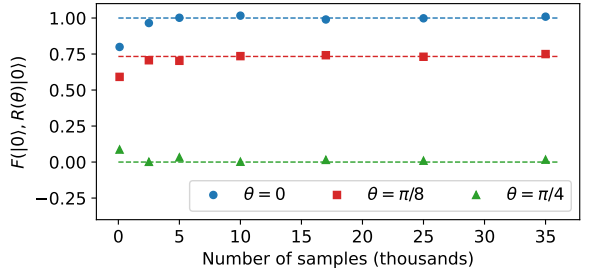
FIG. 3. (a) Absolute error in the estimation of  $F(\text{GHZ}, \mathcal{E}_p(\text{GHZ}))$ , where  $\mathcal{E}_p$  is the depolarizing channel on the first qubit, for different numbers of samples. (b) Estimated fidelity as a function of the number of samples.

Figure 4 shows the fidelity of the  $|0\rangle^{\otimes n}$  state vector with a rotated version  $R(\theta)|0\rangle^{\otimes n}$ , where  $R(\theta)$  is a depth-2 brickwork circuit of two-local unitaries  $U(\theta) = e^{i\theta X \otimes X}$ . As expected the absolute error decreases with the number of samples. For the rotated  $|0\rangle^{\otimes n}$  state vectors in Figure 4, the error is not consistently smaller with more samples, but this is expected. This is because it might happen by chance that a set of snapshots is particularly good at capturing a particular observable, but by looking at a set of observables like in the figure it is apparent that a higher number of samples implies a smaller error for the worst observable, as expected.

Next, we consider the effect locality has on operators with



(a)



(b)

FIG. 4. (a) Absolute error in the estimation of  $F(|0\rangle, R(\theta)|0\rangle)$  for different numbers of samples. (b) Estimated fidelity as a function of the number of samples.

high Frobenius norm. For different weights,  $k$ , Figure 5 shows the absolute error of the estimate with respect to the  $|0\rangle^{\otimes 8}$  state vector for the family of observables  $O_k(\theta) = O(\theta)^{\otimes k} \otimes \mathbb{I}^{8-k}$ , where  $O(\theta) = \cos(\theta)Z + \sin(\theta)X$ . As expected, for small  $k$ , i.e., local observables, the error is manageable, but for higher  $k$  it increases dramatically. To emphasize this point, Figure 6 shows the squared shadow norm of Pauli strings of weight  $k$  as a function of the depth  $d$  for  $n = 20$ .

We can see that there is a sharp drop from  $d = 0$  to  $d = 1$ , and at the intermediate regime most Paulis have a smaller shadow norm than at either extreme, the Paulis that perform worse have a shadow norm that is only slightly larger than the  $d = \infty$  limit, as expected in light of Theorem 11.

## X. DISCUSSION

In this work we provide a protocol for estimating properties of complex quantum systems from randomized measurements. In particular, we consider measurements in a basis generated by random quantum circuits of 2-local Clifford gates of arbitrary depth  $d$ . This ensemble sits between the two extremes proposed in the seminal work Ref. [11]: uniformly random single qubit Clifford unitaries and uniform global Clifford unitaries. We show that the eigenvalues of the corresponding measurement channel have an intuitive interpretation as probabilities and that it is possible to express them as MPS, and provide a variational procedure to obtain a MPS approximating the eigenvalues of the inverse measure-

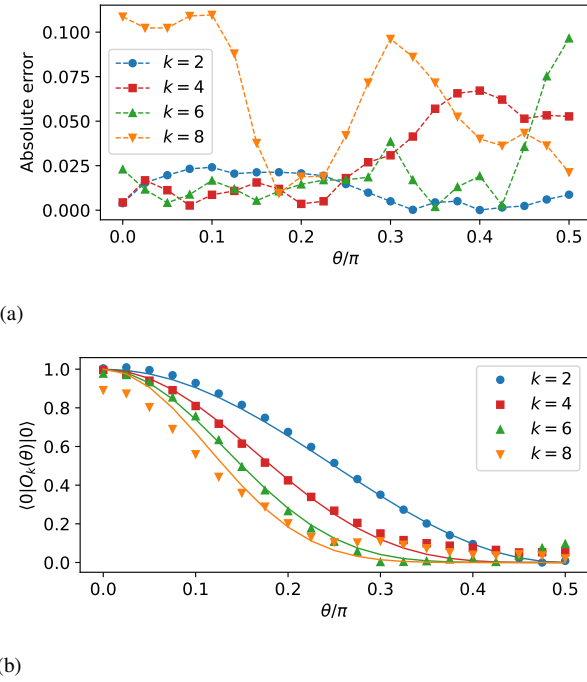


FIG. 5. (a) Absolute error in the estimation of  $\langle 0 |^{⊗n}O_k(\theta)|0\rangle^{⊗n}$  for  $N = 50000$  samples. The estimation becomes less accurate with the support of the observable, suggesting that more samples are required. (b) Estimated expectation value as a function of  $\theta$ . The solid line is the exact value  $\cos(\theta)^k$ .

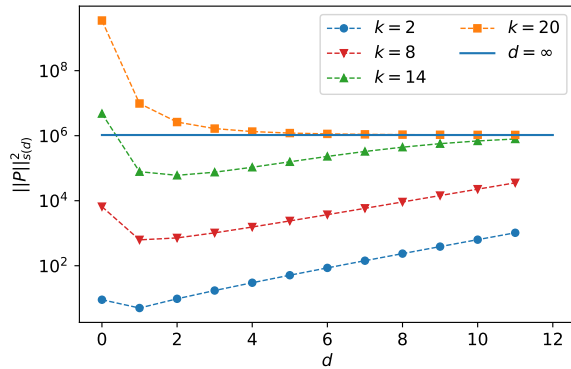


FIG. 6. Squared shadow norm of Pauli strings of different weights  $k$  as a function of depth for  $n = 20$ . A sharp drop is visible from the  $d = 0$  value of  $3^{|P|}$  to the intermediate value  $\sim 2^{|P|+2d}$ , after which we see convergence to the limiting value of  $2^n + 1$  for all Paulis. In the intermediate regime, the shadow norm worst performing Pauli quickly converges to its limiting value.

ment channel. This procedure is heralded in the sense that its accuracy can be verified and the error of the approximation can be efficiently measured. Overall, this allows us to compute expectation values of a large class of experimentally relevant observables, namely, those that can be written as a polynomial bond dimension MPO, as well as to estimate the number of samples necessary to achieve a certain accuracy

in the estimation. Up to the inversion of the measurement channel, which has to be performed only once for any given depth and number of qubits, our protocol is computationally efficient in the regime  $d = \mathcal{O}(\log(n))$ . We gather evidence that in this regime our protocol yields essentially the same guarantees on the sampling complexity as the global Cliffords scheme. In particular, we find that for fully supported observables the locally scrambled shadow norm is essentially the same at a depth  $d \sim \log(n)$  as it is at infinite depth, and at the same time it remains controlled for locally supported observables, which is not true for the global Clifford scheme. This is shown with the same techniques that are used to prove that log-depth random quantum circuits anti-concentrate [27–29], a key property for quantum advantages, and we expect that a similar behaviour is true for the worst-case shadow norm, as this is simply a third moment of the circuit. A rigorous proof of this is much more involved and we leave this to future work. Moreover, it has been shown in Ref. [30] that the ensemble “severely” fails to anti-concentrate at sub-logarithmic depth, we then expect the ensemble at lower depth to have properties closer to the single qubits Cliffords and admit large sample complexity for non-local observables. This behaviour suggests a phase transition from local-to-global happening at log-depth, we then expect this regime to be a “sweet spot” that inherits the benefits of the global Cliffords scheme while requiring much fewer resources, being efficiently implementable, and retaining the desirable locality properties of the local Cliffords schemes.

Many questions and problems remain open: Low bond dimension MPS representations of the inverse measurement channel appear to exist based on numerical evidence, nevertheless, there is to date no theoretical guarantee of their existence, nor of their expected bond dimension. It is expected that a proof of this fact would shed light on a more guided manner of finding the inverse. Furthermore, while our bounds on the locally scrambled shadow norm provide compelling evidence that this protocol is useful at log-depth, a rigorous proof of sample efficiency for large classes of observables is missing. Finally, we provide ways of estimating the sample complexity for individual observables, we are confident that the computations involved in these procedures can be made more efficient by MPS bond dimension reduction techniques.

## XI. ACKNOWLEDGEMENTS

We thank Ingo Roth for fruitful discussions. We also acknowledge a discussion with two groups of researchers: On the one hand, Ahmed A. Akhtar, Hong-Ye Hu, Yi-Zhuang You, and on the other hand Mirko Arienzo, Markus Heinrich, and Martin Kliesch that both independently and concurrently investigated intermediate classical shadows schemes. HP acknowledges the Centre for Quantum Software and Information at the University of Technology Sydney and Michael Bremner for hosting him as a visiting scholar. We thank the BMBF (Hybrid, MuniQC-Atoms, DAQC) the MATH+ Cluster of Excellence, the Einstein Foundation (Einstein Unit on Quantum Devices), the QuantERA (HQCC), the Munich

Quantum Valley (K8), and the DFG (CRC 183, EI 519 20-1, EI 519/21-1) for support.

### Appendix A: Proof of Lemma 1

Let us begin by noting that for all  $d$  (including  $d = 0$  and  $d = \infty$ ) the ensemble  $\mathcal{U}_d$  is Pauli invariant in the sense that for any Pauli  $S \in \mathcal{P}_n$ , and any Clifford  $U \in \mathbb{U}_d$ , we have  $\mu_d(PU) = \mu_d(UP) = \mu_d(U)$ . Let us first prove the following useful result.

**Lemma 12.** *Let  $\mathcal{U}$  be a Pauli invariant ensemble and let  $P_1, \dots, P_k \in \mathcal{P}_n$  be a collection of  $k$  Pauli operators such that  $\prod_{i=1}^k P_i \neq \pm \mathbb{I}$ . Then*

$$\mathbb{E}_{U \sim \mathcal{U}} \left[ \prod_{i=1}^k \langle 0 | UP_i U^\dagger | 0 \rangle \right] = 0. \quad (\text{A1})$$

In addition, if  $\prod_{i=1}^k P_i = \mathbb{I}$ , then

$$\mathbb{E}_{U \sim \mathcal{U}} \left[ \prod_{i=1}^k \langle 0 | UP_i U^\dagger | 0 \rangle \right] = \Pr_{U \sim \mathcal{U}} (\forall i, UP_i U^\dagger \in \pm \mathcal{Z}). \quad (\text{A2})$$

*Proof.* We begin by noticing that for any Pauli  $P$ ,  $\langle 0 | P | 0 \rangle = 0$  unless  $P \in \pm \mathcal{Z}$ , and in this case its value is  $\pm 1$ . This means that unless  $P_1, \dots, P_k$  all commute,  $\prod_{i=1}^k \langle 0 | UP_i U^\dagger | 0 \rangle = 0$  for any Clifford  $U$ , since for this product not to vanish, we must have  $UP_i U^\dagger \in \pm \mathcal{Z}$  for all  $i$ . Since a product of Hermitian commuting matrices is Hermitian,  $\prod_{i=1}^k P_i \neq \pm i \mathbb{I}$ . Suppose  $\prod_{i=0}^k P_i \neq \pm \mathbb{I}$ , and thus  $P_1 \neq \pm P_2 \dots P_k$ , hence, there exists  $Q$  such that  $[P_1, Q] = 0$  and  $\{Q, P_2 \dots P_k\} = 0$ . For  $Q$  to anti-commute with the products of  $P_2$  to  $P_n$ , it must anti-commute with an odd number of them. We then have

$$\mathbb{E}_{U \sim \mathcal{U}} \left[ \prod_{i=1}^k \langle 0 | UP_i U^\dagger | 0 \rangle \right] = \mathbb{E}_{U \sim \mathcal{U}} \left[ \prod_{i=1}^k \langle 0 | UQP_i QU^\dagger | 0 \rangle \right] = - \mathbb{E}_{U \sim \mathcal{U}} \left[ \prod_{i=1}^k \langle 0 | UP_i U^\dagger | 0 \rangle \right], \quad (\text{A3})$$

where we have used Pauli invariance in the second equality. Suppose now  $\prod_{i=0}^k P_i = \mathbb{I}$ . Since  $\prod_{i=1}^k UP_i U^\dagger = \mathbb{I} \in +\mathcal{Z}$ , if  $UP_i U^\dagger \in \pm \mathcal{Z}$  for all  $i$ , only an even number of  $UP_i U^\dagger$  can be in  $-\mathcal{Z}$ , then

$$\prod_{i=1}^k \langle 0 | UP_i U^\dagger | 0 \rangle = \begin{cases} 1 & \text{if } UP_i U^\dagger \in \pm \mathcal{Z} \forall i = 1, \dots, k \\ 0 & \text{otherwise.} \end{cases} \quad (\text{A4})$$

By using the definition of expectation value, we get

$$\mathbb{E}_{U \sim \mathcal{U}} \left[ \prod_{i=1}^k \langle 0 | UP_i U^\dagger | 0 \rangle \right] = \Pr_{U \sim \mathcal{U}} (\forall i, UP_i U^\dagger \in \pm \mathcal{Z}). \quad (\text{A5})$$

□

We now move on to proving Lemma 1.

*Proof.* From Equation (2), we have

$$\mathcal{M}_d(\rho) = \mathbb{E}_{U \sim \mathcal{U}_d} \left[ \sum_{b \in \{0,1\}^n} \langle b | U \rho U^\dagger | b \rangle U^\dagger | b \rangle \langle b | U \right] = 2^n \mathbb{E}_{U \sim \mathcal{U}_d} [\langle 0 | U \rho U^\dagger | 0 \rangle U^\dagger | 0 \rangle \langle 0 | U], \quad (\text{A6})$$

where we have used that the ensemble  $\mathcal{U}_d$  is Pauli invariant and hence every term in the sum must have the same value, since  $|0\rangle$  differs from  $|b\rangle$  only by a Pauli string. For  $P^\lambda, P^{\lambda'} \in \mathcal{P}_n$ , expanding  $\mathcal{M}_d(P)$  in the Pauli basis, we can write the coefficient corresponding to  $P^{\lambda'}$  as

$$\frac{1}{2^n} \text{tr} (P^{\lambda'} \mathcal{M}_d(P^\lambda)) = \mathbb{E}_{U \sim \mathcal{U}_d} [\langle 0 | UP^\lambda U^\dagger | 0 \rangle \langle 0 | UP^{\lambda'} U^\dagger | 0 \rangle]. \quad (\text{A7})$$

By Lemma 12, this vanishes unless  $P^{\lambda'} = \pm P^\lambda$ , but since  $-P^\lambda \notin P_n$ , it vanishes unless  $P^{\lambda'} = P^\lambda$ , then

$$\mathcal{M}(P^\lambda) = t_{\lambda,d} P^\lambda \quad (\text{A8})$$

with, again by Lemma 12,

$$t_{\lambda,d} = \frac{1}{2^n} \text{tr}(P^\lambda \mathcal{M}(P^\lambda)) = \mathbb{E}_{U \sim \mathcal{U}} \left[ \langle 0 | U P^\lambda U^\dagger | 0 \rangle^2 \right] = \Pr_{U \sim \mathcal{U}_d} (U P^\lambda U^\dagger \in \pm \mathcal{Z}). \quad (\text{A9})$$

□

### Appendix B: Proof of Lemma 2

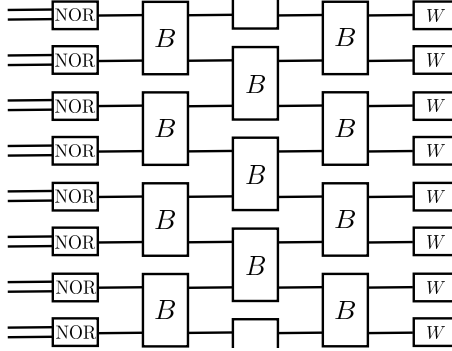


FIG. 7. Tensor network for computing  $t_d(P^\lambda)$  for  $n = 8$  qubits and depth  $d = 3$ . This can be constructed from the random Clifford architecture (c.f. Figure 1) by replacing single qubit random Clifford gates by the NOR gate, replacing 2-qubit random Clifford gates by the  $B$  matrix and ending with a  $W$  vector which evaluates to  $1/3^a$  for index value  $a \in \{0, 1\}$ .

*Proof.* We define the map  $g : \mathcal{P}_n \rightarrow \{0, 1\}^n$  such that the  $k^{\text{th}}$  entry of  $g(P)$  is 0 if and only if the  $k^{\text{th}}$  tensor factor of  $P$  is the identity. We call  $g(P)$  the signature of  $P$ . We note that  $g(P^{(x,z)}) = (\text{NOR}(x_1, z_1), \dots, \text{NOR}(x_n, z_n))$ . From Equation (5) and by noting that the  $0^{\text{th}}$  layer of gates locally scrambles/symmetrizes the Paulis  $X, Y$  and  $Z$ , it is clear that  $t_d(P)$  can only depend on the signature of  $P$ . To construct a tensor network that evaluates  $t_d(P^\lambda)$  (for an input leg assignment of  $\lambda$ ), we first act with NOR gates to map  $\lambda$  to the signature of  $P^\lambda$  (c.f. Figure 7). Then we act with a  $4 \times 4$  real matrix  $B$  in a brickwork pattern corresponding to the locations of the 2-qubit random Clifford gates in the brickwork architecture (c.f. Figure 1). The columns of the matrix  $B$ ,

$$B := \begin{bmatrix} 1 & 0 & 0 & 0 \\ 0 & 0.2 & 0.2 & 0.2 \\ 0 & 0.2 & 0.2 & 0.2 \\ 0 & 0.6 & 0.6 & 0.6 \end{bmatrix},$$

can be interpreted as conditional probability distributions. Indexing the rows and columns of  $B$  by the bit pairs  $g, g' \in \{0, 1\}^2$ , respectively, we interpret  $B_{g,g'}$  as the probability that a uniformly sampled 2-qubit Clifford gate  $U$  conjugates a Pauli with signature  $g'$  to a Pauli with signature  $g$ . Hence, after applying  $d$  layers of  $B$  matrices, if we label the input legs of the tensor network by  $\lambda \in \{0, 1\}^{2n}$  and the output legs by  $\gamma \in \{0, 1\}^n$ , the tensor element will correspond to the probability

$$\Pr_{U \sim \mathcal{U}_d} (g(U P^\lambda U^\dagger) = \gamma).$$

We need to multiply this by the conditional probability

$$\Pr_{U \sim \mathcal{U}_d} (U P^\lambda U^\dagger \in \pm \{\mathbb{I}, Z\}^{\otimes n} \mid g(U P^\lambda U^\dagger) = \gamma)$$

and sum over all  $\gamma$  to arrive at the probability in Equation (5). Checking the condition  $U P^\lambda U^\dagger \in \pm \{\mathbb{I}, Z\}^{\otimes n}$  can be done by checking if each local Pauli factor is either  $\mathbb{I}$  (always the case when its associated signature is 0) or  $Z$ . Given that an output Pauli factors has signature 1, it is a Pauli  $Z$  with probability  $1/3$  over the randomness of  $U$ . This can easily be checked by noting that this property is inherited from the last local (one or two qubit) component of  $U$  to act on the Pauli factor. Thus,  $t_d(P^\lambda)$  (c.f.

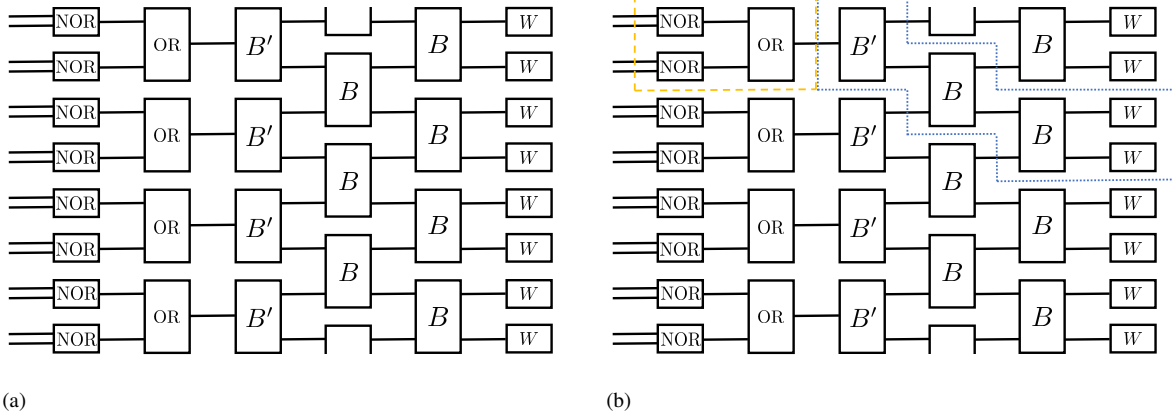


FIG. 8. (a) A simpler tensor network for computing  $t_d(P^\lambda)$  for  $n = 8$  qubits and depth  $d = 3$ . (b) Shows groupings of components that will be used for the form presented in Figure 2.

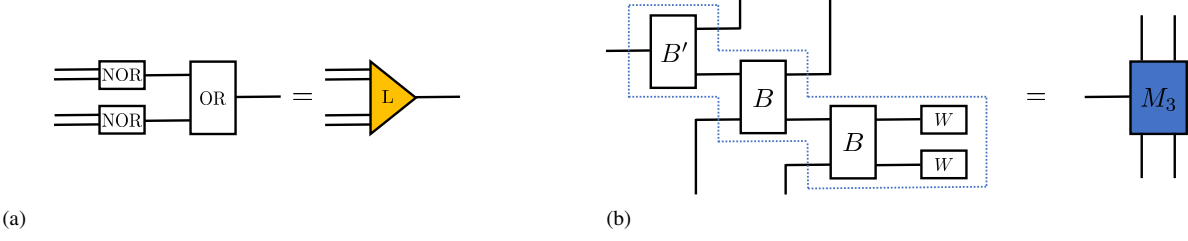


FIG. 9. Representation of grouped components used in Figure 2.

Equation (5)) can be computed by contracting each output leg by the vector  $W = [1 \ 1/3]$  which applies a factor of 1 if the local signature is 0 and a factor of  $1/3$  if the signature is 1. The resulting tensor network evaluates  $t_d(P^\lambda)$ , however, we make some further simplifications. First, we note that since the last three columns of  $B$  are identical,  $B_{g,g'}$  only depends on  $\text{OR}(g')$  in the sense that  $B_{g,g'} = B'_{g,\text{OR}(g')}$  where

$$B' := \begin{bmatrix} 1 & 0 \\ 0 & 0.2 \\ 0 & 0.2 \\ 0 & 0.6 \end{bmatrix}.$$

This simplifies Figure 7 to the tensor network given in Figure 8. Using the definitions presented in Figure 9, we can draw this tensor network as per Figure 2.  $\square$

### Appendix C: Examples of variational inverses

We present here a few examples of variational inverses for  $n = 8$  with  $C(V_0, V_1) = 10^{-5}$  obtained on a laptop computer:

$d = 2$  Time employed: 5 seconds

$$V_0 = \begin{bmatrix} 1 & 0 & 0 \\ 0.20702885 & 0 & 0 \\ 4.77367625 & -1.85042415 & 0 \end{bmatrix}, \quad V_1 = \begin{bmatrix} 0.41248232 & -0.42769035 & 2.11621549 \\ -0.89166157 & -2.16311825 & 0.76938539 \\ 1.94677394 & 0.66783489 & 3.14894043 \end{bmatrix}. \quad (\text{C1})$$

$d = 3$  Time employed: 72 seconds

$$V_0 = \begin{bmatrix} 1 & 0 & 0 \\ 3.93234605 & 0 & 0 \\ 1.53313271 & 1.20626572 & 0 \end{bmatrix}, \quad V_1 = \begin{bmatrix} 2.39842795 & 1.43789702 & 1.46774622 \\ 1.92640124 & 2.19069889 & 0.08802949 \\ 0.85882509 & 0.26351743 & -0.12805757 \end{bmatrix}. \quad (\text{C2})$$

$d = 4$  Time employed: 288 seconds

$$V_0 = \begin{bmatrix} 1 & 0 & 0 & 0 \\ -5.68411434 & 0 & 0 & 0 \\ 2.64486981 & 5.41200524 & 0 & 0 \\ 0.07239611 & -0.10299595 & 0.68939577 & 0 \end{bmatrix}, \quad V_1 = \begin{bmatrix} 2.43664283 & -1.19025024 & -0.62559942 & -0.17076889 \\ -1.19025024 & 3.08122157 & 0.27654966 & -0.13550419 \\ -0.62559942 & 0.27654966 & -0.35425497 & -0.0534837 \\ -0.17076889 & -0.13550419 & -0.0534837 & -0.23622714 \end{bmatrix}. \quad (\text{C3})$$

#### Appendix D: Proof of Lemma 4

*Proof.* For any  $\rho = \sum_{\lambda} \alpha_{\lambda} P^{\lambda}$ , we have

$$\|\mathcal{V} \circ \mathcal{M}(\rho) - \rho\|_F^2 = \left\| \sum_{\lambda} \alpha_{\lambda} P^{\lambda} (t_{\lambda, d} v_d - 1) \right\|_F^2 = \sum_{\lambda} \text{tr}(I) \alpha_{\lambda}^2 (t_{\lambda, d} v_d - 1)^2 \leq \epsilon^2 \|\rho\|_F^2, \quad (\text{D1})$$

which proves, defining  $\tilde{\mathbb{I}} = \mathcal{V} \circ \mathcal{M}$ , that

$$\|\tilde{\mathbb{I}} - \mathbb{I}\|_{\infty} \leq \epsilon. \quad (\text{D2})$$

In particular, consider the approximate classical shadow

$$\tilde{\rho}_s = \mathcal{V}(U^{\dagger} | b_s \rangle \langle b_s | U), \quad (\text{D3})$$

where both  $U$  and  $b_s$  are drawn at random. The expectation value of an observable  $O$  under a classical shadow is

$$\tilde{o}_s(U, b_s) = \text{tr}(O \tilde{\rho}_s). \quad (\text{D4})$$

The average of this quantity over many instances of  $O_s$  is  $\epsilon$  close to the real average of  $O$  under the state  $\rho$

$$\tilde{o} = \mathbb{E}(\text{tr}(O \tilde{\rho}_s)) = \text{tr}(O \mathcal{V}(\mathbb{E}(U^{\dagger} | b_s \rangle \langle b_s | U))) = \text{tr}(O \mathcal{V} \circ \mathcal{M}(\rho)). \quad (\text{D5})$$

Hence, by using Hölder's inequality with  $p = \infty, q = 1$  and that  $\|\rho\|_1 = 1$ ,

$$|\tilde{o} - \text{tr}(O \rho)| = |\text{tr}(O \mathcal{V} \circ \mathcal{M}(\rho)) - \text{tr}(O \rho)| = |\langle O, (\tilde{\mathbb{I}} - \mathbb{I}) \rho \rangle_{HS}| \leq \epsilon \|O\|_{\infty}. \quad (\text{D6})$$

□

#### Appendix E: Proof of Corollary 6

*Proof.* Analogous to the tensor construction of  $t_{\lambda, d}$  given in Figure 2 and Appendix B, here we will construct a tensor network with  $4n$  uncontracted binary legs such that when these are assigned the input  $\lambda, \lambda' \in \{0, 1\}^{2n}$ , the tensor evaluates to  $\tau_{(\lambda, \lambda'), d}$ . We first define three tensors that will be the building blocks of  $\tau_{(\bullet), d}$ .

First, we define  $\Lambda$  a tensor with 4 binary input and 4 binary output legs (that specify a pair of input and a pair of output single qubit Paulis). For  $g, g', h, h' \in \{0, 1\}^2$ , we define  $\Lambda$  by its entries

$$\Lambda_{(h, h'), (g, g')} := \frac{1}{|\mathcal{C}_1|} \sum_{U \in \mathcal{C}_1} \left| \frac{1}{4} \text{tr} \left( (P^h \otimes P^{h'})(U P^g U^{\dagger} \otimes U P^{g'} U^{\dagger}) \right) \right|. \quad (\text{E1})$$

The entry  $\Lambda_{(h, h'), (g, g')}$  can be interpreted as the probability that a pair of Paulis  $(P^g, P^{g'})$  are, under conjugation by  $U$ , mapped to the pair of Paulis  $(P^h, P^{h'})$  up to a factor of  $\pm 1$  when  $U$  is drawn uniformly at random from the set of single qubit Clifford gates  $\mathcal{C}_1$ .

We now define  $\Gamma$ , the two qubit analoge of  $\Lambda$ . Specifically,  $\Gamma$  is a tensor with 8 binary input and 8 binary output legs (that specify a pair of input and a pair of output two qubit Paulis). For  $g, g', h, h' \in \{0, 1\}^4$ , we define  $\Gamma$  by its entries

$$\Gamma_{(h, h'), (g, g')} := \frac{1}{|\mathcal{C}_2|} \sum_{U \in \mathcal{C}_2} \left| \frac{1}{16} \text{tr} \left( (P^h \otimes P^{h'}) (U P^g U^\dagger \otimes U P^{g'} U^\dagger) \right) \right|. \quad (\text{E2})$$

The entry  $\Gamma_{(h, h'), (g, g')}$  can be interpreted as the probability that a pair of 2-qubit Paulis  $(P^g, P^{g'})$  are, under conjugation by  $U$ , mapped to the pair of Paulis  $(P^h, P^{h'})$  up to a factor of  $\pm 1$  when  $U$  is drawn uniformly at random from the set of two qubit Clifford gates  $\mathcal{C}_2$ .

By building a depth  $d$  brickwork (c.f. Figure 1 for  $d = 3$ ) using  $\Lambda$  tensors in the 0<sup>th</sup> layer and  $\Gamma$  tensors in layers  $1, 2, \dots, d$ , we will construct a tensor with  $4n$  input and  $4n$  output legs that for  $(\lambda, \lambda') \in \{0, 1\}^{4n}$  inputs and  $(\nu, \nu') \in \{0, 1\}^{4n}$  outputs evaluates the probability that  $U$  drawn from the ensemble  $\mathcal{U}_d$  will, up to a phase factor of  $\pm 1$ , map  $P^\lambda$  to  $P^\nu$  and simultaneously map  $P^{\lambda'}$  to  $P^{\nu'}$ . To compute  $\tau_{(\lambda, \lambda'), d}$  we simply need to sum over all  $\nu, \nu'$  that are consistent with Pauli strings of  $\mathbb{I}$  and  $Z$ . This can be implemented by a final layer of local  $\Pi$  tensors attached to the brickwork. We now define  $\Pi$ , a tensor with 4 binary input (that specify a pair of single qubit Paulis) and no output legs. For  $g, g' \in \{0, 1\}^2$ , we define  $\Pi$  by its entries

$$\Pi_{(g, g')} := \begin{cases} 1, & \text{if } g_x = g'_x = 0 \\ 0, & \text{otherwise} \end{cases}, \quad (\text{E3})$$

where we use  $g =: (g_x, g_z)$  and  $g' =: (g'_x, g'_z)$  in line with the notation introduced above Equation (1). Intuitively,  $\Pi_{(g, g')}$  evaluates to unity if both input Paulis have no Pauli  $X$  component and zero otherwise. Hence, the tensor product of the local  $\Pi$  tensors only evaluates to unity if the entire Pauli sting consists of a tensor product of  $\mathbb{I}$  and  $Z$  factors. We note that the 0<sup>th</sup> layer of  $\Lambda$  tensors can be omitted when  $d > 0$  since it can be absorbed in to the  $\Gamma$  tensor layer where it acts as a symmetry.

We note that by grouping tensor components in an analogous way to Figure 8, we can write  $\tau_{(\bullet), d}$  as an MPS with bond dimension  $2^{4(d-1)}$ . Some further reductions may be achievable but we leave this to future work. We note that in the  $d = \mathcal{O}(\log n)$  setting, this tensor can be computed efficiently in  $n$  as claimed.  $\square$

## Appendix F: Proofs of performance guarantees

First, we show that the state dependent and locally scrambled shadow norms are actually norms.

**Lemma 13.** *For any state  $\rho$*

$$\|O\|_{s(d), \rho} = \left( \mathbb{E}_{U \sim \mathcal{U}_d} \left[ \sum_{b \in \{0, 1\}^n} \langle b | U \rho U^\dagger | b \rangle \langle b | U \mathcal{M}^{-1}(O) U^\dagger | b \rangle^2 \right] \right)^{1/2}$$

is a norm.

*Proof.* Clearly  $\|O\|_{s(d), \rho}$  is non negative and vanishes for  $O = 0$ . We note that

$$\|O\|_{s(d), \rho}^2 = \langle O, O \rangle_\rho \quad (\text{F1})$$

where

$$\langle A, B \rangle_\rho = \mathbb{E}_{U \sim \mathcal{U}_d} \left[ \sum_{b \in \{0, 1\}^n} \langle b | U \rho U^\dagger | b \rangle \langle b | U \mathcal{M}^{-1}(A) U^\dagger | b \rangle \langle b | U \mathcal{M}^{-1}(B^\dagger) U^\dagger | b \rangle \right] \quad (\text{F2})$$

this expression is symmetric and sesquilinear, hence it is an inner product which induces the state dependent shadow norm, which in turns implies the triangle inequality.  $\square$

The following is then immediate by choosing  $\rho = \mathbb{I}/2^n$ :

**Corollary 14.**  $\|O\|_{s(d), \text{LS}}$  is a norm.

Below are some useful properties of  $\tau_{(\lambda, \lambda')}$  which are self evident from the definition.

**Lemma 15.** *The following hold*

1.  $0 \leq \tau_{(\lambda, \lambda'), d} \leq \min\{t_{\lambda, d}, t_{\lambda', d}, t_{\lambda \oplus \lambda', d}\}$ ,
2.  $\{P^\lambda, P^{\lambda'}\} = 0 \implies \tau_{(\lambda, \lambda'), d} = 0$ ,
3.  $\tau_{(\lambda, \lambda), d} = t_{\lambda, d}$ ,
4.  $\tau_{(\lambda, \lambda'), d} = \tau_{(\lambda', \lambda), d} = \tau_{(\lambda, \lambda \oplus \lambda'), d}$ , and
5. If for all  $U \in \mathcal{U}_d$ ,  $UP^\lambda U^\dagger$  and  $UP^{\lambda'} U^\dagger$  have disjoint support, then  $\tau_{(\lambda, \lambda'), d} = t_{\lambda, d} t_{\lambda', d}$ .

We move on to the proof of Theorem 7.

*Proof.* Expand  $O$  in the expression for the state-dependent shadow norm

$$\begin{aligned} 2^{-n} \|O\|_{s(d), \sigma} &= \sum_{\lambda, \lambda'} \beta_\lambda \beta_{\lambda'} \frac{1}{t_{\lambda, d} t_{\lambda', d}} \mathbb{E}_{U \sim \mathcal{U}_d} \left[ \langle 0 | U \sigma U^\dagger | 0 \rangle \langle 0 | U P^\lambda U^\dagger | 0 \rangle \langle 0 | U P^{\lambda'} U^\dagger | 0 \rangle \right] \\ &= 2^{-n} \sum_{\lambda, \lambda'} \beta_\lambda \beta_{\lambda'} \frac{1}{t_{\lambda, d} t_{\lambda', d}} \mathbb{E}_{U \sim \mathcal{U}_d} \left[ \langle 0 | U P^\lambda U^\dagger | 0 \rangle \langle 0 | U P^{\lambda'} U^\dagger | 0 \rangle \right] \\ &\quad + 2^{-n} \sum_{\lambda, \lambda'} \sum_{\lambda'' \neq 0} \beta_\lambda \beta_{\lambda'} \text{tr} \left( \sigma P^{\lambda''} \right) \frac{1}{t_{\lambda, d} t_{\lambda', d}} \mathbb{E}_{U \sim \mathcal{U}_d} \left[ \langle 0 | U P^\lambda U^\dagger | 0 \rangle \langle 0 | U P^{\lambda'} U^\dagger | 0 \rangle \langle 0 | U P^{\lambda''} U^\dagger | 0 \rangle \right] \end{aligned} \quad (\text{F3})$$

where we have used  $\sigma = 2^{-n} \mathbb{I} + \sum_{\lambda \neq 0} \alpha_\lambda P^\lambda$ . By Lemma 12 and the same argument as in Lemma 1 we have

$$\mathbb{E}_{U \sim \mathcal{U}_d} \left[ \langle 0 | U P^\lambda U^\dagger | 0 \rangle \langle 0 | U P^{\lambda'} U^\dagger | 0 \rangle \right] = \delta_{\lambda, \lambda'} t_{\lambda, d} \quad (\text{F4})$$

and again by Lemma 12 the second term vanished unless  $P^{\lambda''} = \pm P^\lambda P^{\lambda'}$ . Then we have

$$\sum_{\lambda'' \neq 0} \text{tr} \left( \sigma P^{\lambda''} \right) \frac{1}{t_{\lambda, d} t_{\lambda', d}} \mathbb{E}_{U \sim \mathcal{U}_d} \left[ \langle 0 | U P^\lambda U^\dagger | 0 \rangle \langle 0 | U P^{\lambda'} U^\dagger | 0 \rangle \langle 0 | U P^{\lambda''} U^\dagger | 0 \rangle \right] = \text{tr} \left( \sigma P^\lambda P^{\lambda'} \right) \tau_{(\lambda, \lambda'), d} \quad (\text{F5})$$

with

$$\tau_{(\lambda, \lambda'), d} = \mathbb{E}_{U \sim \mathcal{U}_d} (\langle 0 | U P^\lambda U^\dagger | 0 \rangle \langle 0 | U P^{\lambda'} U^\dagger | 0 \rangle \langle 0 | U P^\lambda P^{\lambda'} U^\dagger | 0 \rangle) = \Pr_{U \sim \mathcal{U}_d} (U P^\lambda U^\dagger, U P^{\lambda'} U^\dagger \in \pm \mathcal{Z}), \quad (\text{F6})$$

where we have used Lemma 12 again in the last equality. We then have

$$\|O\|_{s(d), \sigma}^2 = \sum_{\lambda} \frac{\beta_\lambda^2}{t_{\lambda, d}} + \text{tr} \left( \sigma \sum_{\lambda \neq \lambda'} \beta_\lambda \beta_{\lambda'} \frac{\tau_{(\lambda, \lambda'), d}}{t_{\lambda, d} t_{\lambda', d}} P^\lambda P^{\lambda'} \right) = \sum_{\lambda} \frac{\beta_\lambda^2}{t_{\lambda, d}} + \text{tr} \left( \sigma \tilde{O} \right). \quad (\text{F7})$$

It remains to identify the first term as the locally scrambled shadow norm, to see this, notice that

$$\mathbb{E}_{\sigma \sim \mathcal{E}} \left[ \text{tr} \left( \sigma \tilde{O} \right) \right] = \frac{1}{2^n} \text{tr} \left( \tilde{O} \right) = 0. \quad (\text{F8})$$

□

Next, we prove Lemma 10.

*Proof.* Notice that by Hölder's inequality  $\text{tr} \left( \sigma \tilde{O} \right) \leq \|\sigma\|_1 \|\tilde{O}\|_\infty = \|\tilde{O}\|_\infty$ . We have

$$\tilde{O} = \sum_{\substack{\lambda', \lambda \in \{0, 1\}^{2n} \\ \lambda' \neq \lambda}} P^\lambda P^{\lambda'} \beta_\lambda \beta_{\lambda'} \frac{\tau_{(\lambda, \lambda'), d}}{t_{\lambda, d} t_{\lambda', d}}. \quad (\text{F9})$$

Make the change of variables  $\theta = \lambda \oplus \lambda'$  to get

$$\tilde{O} = \sum_{\theta \neq 0} P^\theta \sum_{\lambda} \beta_{\theta \oplus \lambda} \beta_\lambda \frac{\tau_{(\theta \oplus \lambda, \lambda), d}}{t_{\theta \oplus \lambda, d} t_{\lambda, d}}. \quad (\text{F10})$$

The second bound is then simply obtained by the triangle inequality and  $\|P^\theta\|_\infty = 1$ . Finally, notice that

$$\|\tilde{O}\|_\infty \leq \|\tilde{O}\|_F = 2^{n/2} \sqrt{\sum_{\theta \neq 0} \left| \sum_{\lambda} \beta_{\theta \oplus \lambda} \beta_\lambda \frac{\tau_{(\theta \oplus \lambda, \lambda), d}}{t_{\theta \oplus \lambda, d} t_{\lambda, d}} \right|^2}. \quad (\text{F11})$$

□

### Appendix G: Recovering the $d = \infty$ case

It is useful to briefly discuss how to recover the analytical results of Ref. [11] in the  $d = \infty$  case from ours. We already argued that in this case,  $t_{\lambda, \infty}$  does not depend on  $\lambda$  and  $t_{\lambda, \infty} = (2^n + 1)^{-1}$ . To compute  $\tau_{(\lambda, \lambda'), \infty}$  this we will use some machinery for the computation of averages over the unitary group, the following is a direct consequence of Schur's lemma [31]

**Lemma 16.** *Let  $\mu(q)$  be the Haar measure over the unitary group in  $q$  dimensions  $U(q)$ , then for any operator  $X$  on  $(\mathbb{C}^q)^{\otimes k}$  and state  $|\psi\rangle \in \mathbb{C}^q$ ,*

$$\mathbb{E}_{U \sim \mu(q)} [\langle \psi |^{\otimes k} U^{\otimes k} X U^\dagger | \psi \rangle^{\otimes k}] = \binom{q+k-1}{k}^{-1} \text{tr}(\Pi_{\text{sym}} X) \quad (\text{G1})$$

where  $\Pi_{\text{sym}} = \frac{1}{k!} \sum_{\sigma \in S_k} r(\sigma)$  is the projector onto the completely symmetric subspace of  $(\mathbb{C}^q \otimes \mathbb{C}^q)^{\otimes k}$ . Here  $r(\sigma) : |i_1 \dots i_k\rangle \mapsto |i_{\sigma^{-1}(1)} \dots i_{\sigma^{-1}(k)}\rangle$ .

This, coupled with the observation that a brickwork random Clifford circuit forms a 3–design at infinite depth, allows us to readily prove the following lemma.

**Lemma 17.** *For all  $\lambda \neq \lambda', \lambda, \lambda' \neq 0$*

$$\tau_{(\lambda, \lambda'), \infty} = \begin{cases} \frac{2}{(2^n+1)(2^n+2)} & \text{if } [P^\lambda, P^{\lambda'}] = 0 \\ 0 & \text{otherwise.} \end{cases} \quad (\text{G2})$$

*Proof.* Manipulating Equation (F6) we get

$$\begin{aligned} \tau_{(\lambda, \lambda'), \infty} &= \mathbb{E}_{U \sim \mu(2^n)} [\langle 0 |^{\otimes 3} U^{\otimes 3} P^\lambda \otimes P^{\lambda'} \otimes P^\lambda P^{\lambda'} U^\dagger | 0 \rangle^{\otimes 3}] \\ &= \frac{1}{2^n(2^n+1)(2^n+2)} \sum_{\sigma \in S_3} \text{tr} (r(\sigma) P^\lambda \otimes P^{\lambda'} \otimes P^\lambda P^{\lambda'}). \end{aligned} \quad (\text{G3})$$

Notice that for any  $\sigma \in S_3$  that leaves any of the three elements invariant we will have  $\text{tr}(r(\sigma) P^\lambda \otimes P^{\lambda'} \otimes P^\lambda P^{\lambda'}) = 0$ . The only two surviving permutation in the sum are then the two full cycles  $c_1$  and  $c_2$ ,

$$\begin{aligned} \text{tr}(r(c_1) P^\lambda \otimes P^{\lambda'} \otimes P^\lambda P^{\lambda'}) &= \text{tr}(P^\lambda P^{\lambda'} P^\lambda P^{\lambda'}) = 2^n, \\ \text{tr}(r(c_2) P^\lambda \otimes P^{\lambda'} \otimes P^\lambda P^{\lambda'}) &= \text{tr}(P^\lambda P^\lambda P^{\lambda'} P^{\lambda'}) = \pm 2^n, \end{aligned} \quad (\text{G4})$$

where the second sign is positive if the two Paulis commute. This implies the result. □

This allows us to see that in the  $d = \infty$ , the locally scrambled shadow norm is dominant, as a matter of fact in this case we have for  $\lambda \neq \lambda', \lambda, \lambda' \neq 0$

$$\frac{\tau_{(\lambda, \lambda'), d}}{t_{\lambda, d} t_{\lambda', d}} = 2 \frac{2^n + 1}{2^n + 2} < 2. \quad (\text{G5})$$

Using Theorem 7 we can then see that for traceless  $O$

$$\begin{aligned} \|O\|_{s(\infty), \text{LS}}^2 &= \frac{2^n + 1}{2^n} \|O\|_F^2 \\ \text{tr}(\sigma \tilde{O}) &\leq \|\tilde{O}\|_\infty \leq 2 \left\| O^2 - \frac{\mathbb{I}}{2^n} \|O\|_F^2 \right\|_\infty \leq 2 \|O^2\|_\infty + 2 \frac{1}{2^n} \|O\|_F^2 \leq 2 \|O\|_F^2 \leq 2 \|O\|_{s(\infty), \text{LS}}^2. \end{aligned} \quad (\text{G6})$$

## Appendix H: Proof of Theorem 11

We will prove the following statement.

**Lemma 18.** For  $d \geq \Omega(\log(n))$ ,

$$t_{\lambda,d} \geq \frac{1}{2^{\min\{|\lambda|+2d,n\}}+1} \frac{1}{1+\frac{1}{n^{\mathcal{O}(1)}}} \quad (\text{H1})$$

where  $|\lambda|$  is the maximum distance between any two qubits where  $P^\lambda$  is supported.

Combining this with the expression for the shadow norm, we obtain Theorem 11. More specifically, we have that if  $d \geq \Omega(\log(n))$

$$\|O\|_{s(d),\text{LS}}^2 = \sum_{\lambda} \frac{\beta_{\lambda}^2}{t_{\lambda,d}} \leq \left(1+n^{-\Omega(1)}\right) (2^n+1) \sum_{\lambda} \beta_{\lambda}^2 = \left(1+n^{-\Omega(1)}\right) \frac{2^n+1}{2^n} \|O\|_F^2 \quad (\text{H2})$$

and if  $d = \Theta(\log(n))$ ,  $|\lambda| \leq \mathcal{O}(\log(n))$ , we have

$$\frac{1}{t_{\lambda,d}} \leq \frac{n^{\mathcal{O}(1)}}{1+\frac{1}{n^{\mathcal{O}(1)}}} = n^{\mathcal{O}(1)}, \quad (\text{H3})$$

hence if  $O$  only contains Paulis such that  $|\lambda| \leq \mathcal{O}(\log(n))$ , we get

$$\|O\|_{s(d),\text{LS}}^2 = \sum_{\lambda} \frac{\beta_{\lambda}^2}{t_{\lambda,d}} \leq n^{\mathcal{O}(1)} \sum_{\lambda} \beta_{\lambda}^2 = n^{\mathcal{O}(1)} 2^{-n} \|O\|_F^2. \quad (\text{H4})$$

To prove Lemma 18, we rely on a well known mapping from moments of random quantum circuits to a path counting problem [32–34] which we only briefly summarize. For an in depth derivation, we direct the reader to Ref. [34]. We have

$$\mathbb{E}_{U \sim \mathcal{U}} \langle 0 | U P U^\dagger | 0 \rangle^2 = \mathbb{E}_{U \sim \mathcal{U}} \langle P | U^{\otimes 2} \otimes \bar{U}^{\otimes 2} | 0 \rangle^{\otimes 4} \quad (\text{H5})$$

where  $|P\rangle$  is the vectorization of the Pauli  $P$  and  $U$  is a random depth  $d$  Clifford circuit. The average over the circuit is simply the average over the individual two-local gates, which can be seen as drawn from the Haar measure of the unitary group in dimension 4,  $\mu_H(4)$ , since the Clifford group forms a unitary 3-design [35]. Using a tool known as *Weingarten calculus* [36, 37], an application of Schur-Weyl duality, we can write

$$\mathbb{E}_{U \sim \mu_H(4)} U^{\otimes 2} \otimes \bar{U}^{\otimes 2} = \sum_{\sigma \in S_2} \text{Wg}(\sigma^{-1} \tau, 4) |\sigma\rangle \langle \tau| \quad (\text{H6})$$

where  $S_2$  is the permutation group of two elements,  $\text{Wg}$  is the Weingarten function, and for  $\sigma \in S_2$   $|\sigma\rangle$  is the vectorization of the operator on  $\mathbb{C}^4$  which permutes the 4 tensor product elements as  $\sigma$ . Graphically, we can represent this equation as follows

$$\mathbb{E} \begin{array}{c} \text{light box} \\ \text{dark box} \end{array} = \sum_{\sigma \in S_2} \begin{array}{c} \text{black circle} \\ \text{red circle} \end{array} \begin{array}{c} \text{outgoing leg} \\ \text{ingoing leg} \end{array} \quad (\text{H7})$$

Here, the light boxes represent the two copies of  $U$  and the dark boxes the two copies of  $\bar{U}$ , the black and red circles represent choices of permutations. The outgoing and ingoing legs are permutation vectorizations, the leg connecting the two permutations represents the Weingarten function  $\text{Wg}(\sigma^{-1} \tau, 4)$ . Applying this to the whole circuit, we get the sum over all black and red circles in the hexagonal lattice in Figure 10. This is reminiscent of the partition function of a statistical mechanics model in which the spins are given by choices of permutations, and the interactions are given by either Weingarten functions or overlaps of permutation vectorizations, performing this sum becomes substantially simpler if we first sum over all red circles, we then get an equivalent model on a triangular lattice

$$\sum_{\sigma_3} \begin{array}{c} \text{black circle} \\ \text{red circle} \end{array} = \sigma_3 \cdot \begin{array}{c} \text{triangle} \\ \bullet^{\sigma_1} \\ \bullet^{\sigma_2} \end{array} = \begin{cases} 1 & \text{if } \sigma_1 = \sigma_2 = \sigma_3 \\ \frac{2}{5} & \text{if } \sigma_1 = \sigma_3, \sigma_2 = \sigma_3 \\ 0 & \text{otherwise} \end{cases} \quad (\text{H8})$$

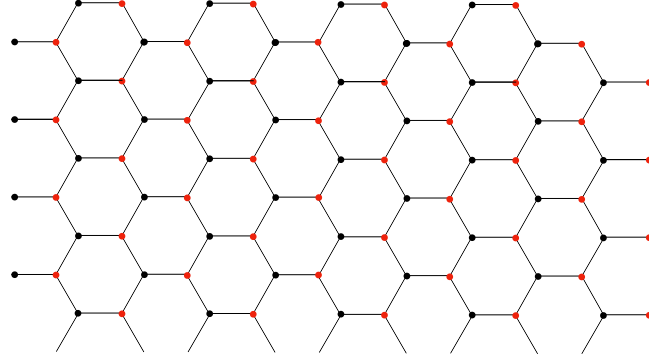


FIG. 10. Summing over all black and red circles in this hexagonal lattice corresponds to averaging over all two-local gates in the brickwork random quantum circuit.

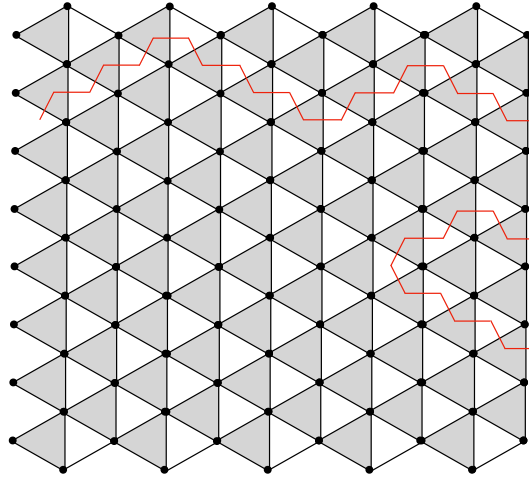


FIG. 11. Triangular lattice with two domain walls.

sums over vertices in this new triangular model can be seen as sums over domain walls between regions of identity and flip permutations, each domain wall of length  $l$  has a weight of  $(2/5)^l$ . Figure 11 shows the triangular lattice with an example of a two domain walls configuration. We still have to discuss the boundary condition. On the right boundary every permutation is contracted with the vector  $|0\rangle^4$ , and  $\langle\sigma|0,0,0,0\rangle = 1$ . We still have to sum over the red circles at the right boundary, the value of this sum is independent of the neighboring black circle and from the whole right boundary, we get

$$(\text{Wg}(\mathbb{1}, 4) + \text{Wg}(F, 4))^{n/2} = \frac{1}{\sqrt{5}^n} \quad (\text{H9})$$

for every boundary spin, where  $\mathbb{1}, F \in S_2$  are the identity and flip permutation respectively. The left boundary is more interesting. For a non trivial Pauli, we have

$$\langle \mathbb{1} | (|P\rangle)^{\otimes 2} = \text{tr}(P)^2 = 0 \quad \langle F | (|P\rangle)^{\otimes 2} = \text{tr}(P^2) = 2. \quad (\text{H10})$$

For the identity, instead we have

$$\langle \mathbb{1} | (|\mathbb{I}\rangle)^{\otimes 2} = 4 \quad \langle F | (|\mathbb{I}\rangle)^{\otimes 2} = 2. \quad (\text{H11})$$

Hence, wherever there is a non trivial Pauli at the left hand boundary, only the flip permutation is allowed. We are now ready to lower bound  $t_{\lambda, d}$ . First of all, notice that if  $P^\lambda = P \otimes \mathbb{I}$  is not fully supported

$$t_{\lambda, d} = \mathbb{E}_{U \sim \mathcal{U}_d} [\langle 0 | UP \otimes \mathbb{I} U^\dagger | 0 \rangle^2] \geq \mathbb{E}_{U \sim \mathcal{U}_d} [\langle 0 | UP \otimes QU^\dagger | 0 \rangle^2] \quad (\text{H12})$$

for any Pauli  $Q$ , since  $Q < \mathbb{I}$  as operators. Hence for a lower bound we just need to lower bound  $t_{\lambda,d}$  for fully supported  $P^\lambda$ . We then have

$$t_{\lambda,d} = \left(\frac{2}{\sqrt{5}}\right)^n \sum_{p \in \text{paths}(d)} \text{weight}(p) \quad (\text{H13})$$

since the left boundary is constrained to be comprised entirely of flip permutations, there cannot be any domain walls reaching it, hence all the paths in the sum must begin and end at the right boundary.  $\text{paths}(d)$  are all paths that do not reach beyond a distance  $d$  from the right boundary. We have

$$\begin{aligned} t_{\lambda,\infty} &= \left(\frac{2}{\sqrt{5}}\right)^n \sum_{p \in \text{paths}(\infty)} \text{weight}(p) \leq \left(\frac{2}{\sqrt{5}}\right)^n \sum_{p \in \text{paths}(d)} \text{weight}(p) \left(1 + \sum_{p \in \text{paths}(>d)} \text{weight}(p)\right) \\ &=: t_{\lambda,d} \left(1 + \sum_{p \in \text{paths}(>d)} \text{weight}(p)\right) \end{aligned} \quad (\text{H14})$$

where  $\text{paths}(>d)$  are all paths that reach beyond a distance  $d$  from the left boundary, and we have used that a configuration containing both paths that stay within a distance  $d$  from the boundary and paths that do not has a weight equal to the product of the weights of these two paths. See Figure 12. We then need to upper bound this sum. We have

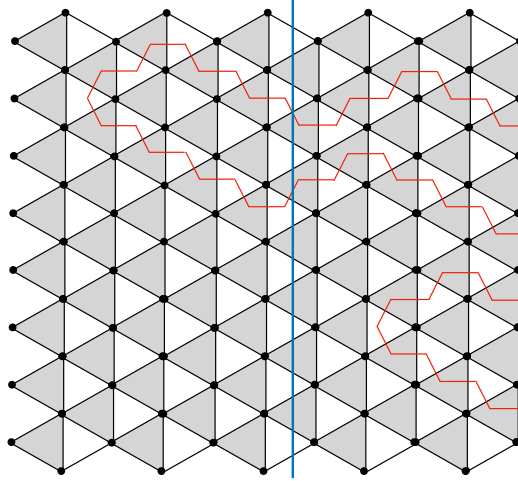


FIG. 12. Two paths beginning and ending at the right boundary, the blue line represents the depth  $d$ , the longer path is not counted in  $t_{\lambda,d}$ , but it is in  $t_{\lambda,\infty}$ , where the weight of this configuration is the product of the weights of the two paths.

$$\sum_{p \in \text{paths}(>d)} \text{weight}(p) = \sum_{t>d} R(t). \quad (\text{H15})$$

Where  $R(t)$  is the sum of all configurations that only contain paths that reach beyond a distance  $t$  from the right boundary and contain at least one path reaching exactly a distance  $t$ . Consider all paths reaching some distance  $t$  from the boundary: each of these paths can go either up or down at every of the  $t$  steps from the boundary to the turn around point, and similarly for the way back to the boundary. Then for every choice of turn around point at a distance  $t$  from the boundary there are fewer than  $2^{2t}$  paths, since there are  $n/2$  possible turn around points, we conclude that there are at most  $n/2 2^{2t}$  of these paths, and each of them has a weight  $(2/5)^{2t}$ . We then have

$$R(t) \leq \frac{n}{2} \left(\frac{4}{5}\right)^{2t} \sum_{m=0}^{\infty} \left(\frac{n}{2}\right)^m \left(\sum_{w=t}^{\infty} \left(\frac{4}{5}\right)^{2w}\right)^m. \quad (\text{H16})$$

In the above expression the case  $m = 0$  represents one path reaching a distance  $t$  from the boundary, and the other terms contain that one path plus  $m$  other paths that may reach a distance  $t$  or higher from the boundary. There can clearly be at most  $n/2$  such

non overlapping paths in a given configuration, but summing to infinity is good enough for our purposes, as the leftover sum will be exponentially small in  $n$ ,

$$\begin{aligned} R(t) &\leq \frac{n}{2} \left(\frac{4}{5}\right)^{2t} \sum_{m=0}^{\infty} \left(\frac{n}{2}\right)^m \left(\sum_{w=t}^{\infty} \left(\frac{4}{5}\right)^{2w}\right)^m = \frac{n}{2} \left(\frac{4}{5}\right)^{2t} \sum_{m=0}^{\infty} \left(\frac{n}{2}\right)^m \left(\frac{4}{5}\right)^{2t} \left(\frac{(4/5)^{2t}}{1 - (4/5)^2}\right)^m \\ &= \frac{n}{2} \left(\frac{4}{5}\right)^{2t} \sum_{m=0}^{\infty} \left(\frac{25}{18} \left(\frac{4}{5}\right)^{2t} n\right)^m. \end{aligned} \quad (\text{H17})$$

Now suppose that

$$d \geq \frac{\alpha \log(n) + \log(1/c)}{\log(16/25)} \quad (\text{H18})$$

for some  $\alpha > 1, c > 0$ , then  $\left(\frac{16}{25}\right)^t \leq cn^{-\alpha}$  and for  $n > \left(\frac{25}{18}c\right)^{\frac{1}{\alpha-1}}$ , we have

$$R(t) \leq \frac{n}{2} \left(\frac{4}{5}\right)^{2t} \sum_{m=0}^{\infty} \left(c \frac{25}{18} n^{1-\alpha}\right)^m = \frac{n}{2} \left(\frac{4}{5}\right)^{2t} \frac{1}{1 - c \frac{25}{18} n^{1-\alpha}} \quad (\text{H19})$$

we then have

$$\sum_{p \in \text{paths}(>d)} \text{weight}(p) \leq \sum_{t>d} R(t) \leq \frac{1}{1 - c \frac{25}{18} n^{1-\alpha}} \frac{25}{18} n \left(\frac{4}{5}\right)^{2(d+1)} \leq \frac{16}{25} \frac{1}{\frac{18}{25c} n^{\alpha-1} - 1}. \quad (\text{H20})$$

Putting everything together, we have

$$t_{\lambda,d} \geq t_{\lambda,\infty} \frac{1}{1 + \frac{16}{25} \frac{1}{\frac{18}{25c} n^{\alpha-1} - 1}} \quad (\text{H21})$$

Suppose now that  $P^\lambda$  is fully supported only on a subregion of the chain of length  $p < n - 2d$ . Let us make the notation more specific and call  $t_{\lambda,d}(n)$  the value of  $t_{\lambda,d}$  on a system of size  $n$ . In this case we can see that  $t_{\lambda,d}(n) = t_{\lambda,d}(n')$  with  $n' = p + 2d < n$ , as the unitaries acting outside the light-cone of a radius  $d$  around the support of the Pauli play no role. The same exact argument as earlier applies, the only difference is the limiting value

$$t_{\lambda,d}(n) = t_{\lambda,d}(n') \geq \frac{1}{2^{p+2d} + 1} \frac{1}{1 + \frac{16}{25} \frac{1}{\frac{18}{25c} n^{\alpha-1} - 1}}. \quad (\text{H22})$$

We can even make the bound better by noticing that the factor  $n$  in  $n^{1-\alpha}$  came from counting the number of possible turn around points for the paths, which in the case of  $t_{\lambda,d}(n')$  is  $n'$  instead. So if we have, in addition to Equation (H18),  $p + 2d \leq r \log(n)$ , and hence  $d = \Theta(\log n)$ , we can replace  $n^{\alpha-1}$  with  $\frac{n^\alpha}{r \log(n)}$  in the bound above.

- [1] R. O'Donnell and J. Wright, "Efficient quantum tomography," in *Proceedings of the Forty-Eighth Annual ACM Symposium on Theory of Computing*, STOC '16 (Association for Computing Machinery, New York, NY, USA, 2016) p. 899–912.
- [2] J. Haah, A. W. Harrow, Z. Ji, X. Wu, and N. Yu, "Sample-optimal tomography of quantum states," in *Proceedings of the Forty-Eighth Annual ACM Symposium on Theory of Computing*, STOC '16 (Association for Computing Machinery, New York, NY, USA, 2016) p. 913–925.
- [3] J. Eisert, D. Hangleiter, N. Walk, I. Roth, D. Markham, R. Parekh, U. Chabaud, and E. Kashefi, "Quantum certification and benchmarking," *Nature Rev. Phys.* **2**, 382–390 (2020).
- [4] M. Kliesch and I. Roth, "Theory of quantum system certification," *PRX Quantum* **2**, 010201 (2021).
- [5] M. G. D'Ariano, M. G. Paris, M. Sacchi, and F. Massimiliano, "Quantum tomography," *Adv. Imag. Elec. Phys.* **128**, 205–308 (2003).
- [6] J. I. Cirac and P. Zoller, "Goals and opportunities in quantum simulation," *Nature Phys.* **8**, 264 (2012).
- [7] D. Gross, Y.-K. Liu, S. T. Flammia, S. Becker, and J. Eisert, "Quantum state tomography via compressed sensing," *Phys. Rev. Lett.* **105**, 150401 (2010).
- [8] M. Cramer, M. B. Plenio, S. T. Flammia, R. Somma, D. Gross, S. Bartlett, O. Landon-Cardinal, D. Poulin, and Y.-K. Liu, "Efficient quantum state tomography," *Nature Comm.* **1**, 149 (2010).

- [9] M. Ohliger, V. Nesme, and J. Eisert, “Efficient and feasible state tomography of quantum many-body systems,” *New J. Phys.* **15**, 015024 (2013).
- [10] S. Aaronson, “Shadow tomography of quantum states,” in *Proceedings of the 50th Annual ACM SIGACT Symposium on Theory of Computing*, STOC 2018 (Association for Computing Machinery, New York, NY, USA, 2018) p. 325–338.
- [11] H.-Y. Huang, R. Kueng, and J. Preskill, “Predicting many properties of a quantum system from very few measurements,” *Nature Phys.* **16**, 1050–1057 (2020).
- [12] T. Brydges, A. Elben, P. Jurcevic, B. Vermersch, C. Maier, B. P. Lanyon, P. Zoller, R. Blatt, and C. F. Roos, “Probing Rényi entanglement entropy via randomized measurements,” *Science* **364**, 260–263.
- [13] A. Elben, B. Vermersch, M. Dalmonte, J. I. Cirac, and P. Zoller, “Rényi Entropies from random quenches in atomic Hubbard and spin models,” *Phys. Rev. Lett.* **120**, 050406 (2018).
- [14] J. Helsen, M. Ioannou, I. Roth, J. Kitzinger, E. Onorati, A. H. Werner, and J. Eisert, “Estimating gate-set properties from random sequences,” (2021), [arXiv:2110.13178](https://arxiv.org/abs/2110.13178).
- [15] A. Elben, S. T. Flammia, H.-Y. Huang, R. Kueng, J. Preskill, B. Vermersch, and P. Zoller, “The randomized measurement toolbox,” (2022), [arXiv:2203.11374](https://arxiv.org/abs/2203.11374).
- [16] G. I. Struchalin, Y. A. Zagorovskii, E. V. Kovlakov, S. S. Straupe, and S. P. Kulik, “Experimental estimation of quantum state properties from classical shadows,” *PRX Quantum* **2**, 010307 (2021).
- [17] A. Elben, R. Kueng, H.-Y. Huang, R. van Bijnen, C. Kokail, M. Dalmonte, P. Calabrese, B. Kraus, J. Preskill, P. Zoller, and B. Vermersch, “Mixed-state entanglement from local randomized measurements,” *Phys. Rev. Lett.* **125**, 200501 (2020).
- [18] T. Zhang, J. Sun, X.-X. Fang, X.-M. Zhang, X. Yuan, and H. Lu, “Experimental quantum state measurement with classical shadows,” *Phys. Rev. Lett.* **127**, 200501 (2021).
- [19] K. Bu, D. E. Koh, R. J. Garcia, and A. Jaffe, “Classical shadows with Pauli-invariant unitary ensembles,” (2022), [arXiv:2202.03272](https://arxiv.org/abs/2202.03272).
- [20] H.-Y. Hu, S. Choi, and Y.-Z. You, “Classical shadow tomography with locally scrambled quantum dynamics,” (2021), [arXiv:2107.04817](https://arxiv.org/abs/2107.04817).
- [21] A. A. Akhtar, H.-Y. Hu, and Y.-Z. You, “Scalable and flexible classical shadow tomography with tensor networks,” (2022), [arXiv:2209.02093](https://arxiv.org/abs/2209.02093).
- [22] G. Lugosi and S. Mendelson, “Mean estimation and regression under heavy-tailed distributions: A survey,” *Found. Comp. Math.* **19**, 1145–1190 (2019).
- [23] M. Lerasle, “Lecture notes: Selected topics on robust statistical learning theory,” (2019), [arXiv:1908.10761](https://arxiv.org/abs/1908.10761).
- [24] F. G. S. L. Brandao, A. W. Harrow, and M. Horodecki, “Local random quantum circuits are approximate polynomial-designs,” *Commun. Math. Phys.* **346**, 397–434 (2016).
- [25] Y. Guo and S. Yang, “Quantum error mitigation via matrix product operators,” (2022), [arXiv:2201.00752](https://arxiv.org/abs/2201.00752).
- [26] N. Hunter-Jones, “Unitary designs from statistical mechanics in random quantum circuits,” (2019), [arXiv:1905.12053](https://arxiv.org/abs/1905.12053).
- [27] A. M. Dalzell, N. Hunter-Jones, and F. G. S. L. Brandão, “Random quantum circuits anticoncentrate in log depth,” *PRX Quantum* **3**, 010333 (2022).
- [28] B. Barak, C.-N. Chou, and X. Gao, “Spoofing linear cross-entropy benchmarking in shallow quantum circuits,” (2020), [arXiv:2005.02421](https://arxiv.org/abs/2005.02421).
- [29] D. Hangleiter and J. Eisert, “Computational advantage of quantum random sampling,” (2022), [arXiv:2206.04079](https://arxiv.org/abs/2206.04079).
- [30] A. Deshpande, B. Fefferman, A. V. Gorshkov, M. J. Gullans, P. Niroula, and O. Shtanko, “Tight bounds on the convergence of noisy random circuits to uniform,” (2021), [arXiv:arXiv:2112.00716](https://arxiv.org/abs/arXiv:2112.00716).
- [31] A. W. Harrow, “The church of the symmetric subspace,” (2013), [arXiv:1308.6595](https://arxiv.org/abs/1308.6595).
- [32] A. Nahum, S. Vijay, and J. Haah, “Operator spreading in random unitary circuits,” *Phys. Rev. X* **8**, 021014 (2018).
- [33] T. Zhou and A. Nahum, “Emergent statistical mechanics of entanglement in random unitary circuits,” *Phys. Rev. B* **99**, 174205 (2019).
- [34] N. Hunter-Jones, “Unitary designs from statistical mechanics in random quantum circuits,” (2019), [arXiv:1905.12053](https://arxiv.org/abs/1905.12053).
- [35] H. Zhu, “Multiqubit Clifford groups are unitary 3-designs,” *Phys. Rev. A* **96**, 062336 (2017).
- [36] P. W. Brouwer and C. W. J. Beenakker, “Diagrammatic method of integration over the unitary group, with applications to quantum transport in mesoscopic systems,” *J. Math. Phys.* **37**, 4904–4934 (1996).
- [37] B. Collins and P. Śniady, “Integration with respect to the Haar measure on unitary, orthogonal and symplectic group,” *Commun. Math. Phys.* **264**, 773–795 (2006).